Eastern Mediterranean volcanism during Marine Isotope Stages 9 to 7e (335–235 ka): Insights based on cryptotephra layers at Tenaghi Philippon, Greece

Polina Vakhrameeva[1], Sabine Wulf[1,2], Andreas Koutsodendris[1], Rik Tjallingii[3], William J. Fletcher[4], Oona Appelt[5], Thomas Ludwig[1], Maria Knipping[6], Mario Trieloff[1], Jörg Pross[1]

[1] Institute of Earth Sciences, Heidelberg University, Im Neuenheimer Feld 234–236, D-69120 Heidelberg, Germany

[2] Department of Geography, University of Portsmouth, Buckingham Building, Lion Terrace, Portsmouth, PO1 3HE, United Kingdom

[3] GFZ German Research Centre for Geosciences, Section 4.3 Climate Dynamics and Landscape Evolution, Telegrafenberg, D-14473 Potsdam, Germany

[4] Department of Geography, School of Environment, Education and Development, University of Manchester, Manchester, M13 9PL, United Kingdom

[5] GFZ German Research Centre for Geosciences, Section 3.6 Chemistry and Physics of Earth Materials, Telegrafenberg, D-14473 Potsdam, Germany

[6] Institute of Botany, University of Hohenheim, Garbenstraße 30, D-70593 Stuttgart, Germany

* Corresponding author: polina.vakhrameeva@geow.uni-heidelberg.de (P. Vakhrameeva)

Keywords: Cryptotephra; Italian and Aegean Arc volcanism; Marine Isotope Stages 9, 8 and 7; Eastern Mediterranean region; Tenaghi Philippon

Abstract

Tephra layers preserved in distal sedimentary archives represent chronicles of explosive volcanism that can complement the often more fragmentary information from near-source volcanic deposits to establish complete volcanic histories. With regard to these aspects, the Middle Pleistocene of the Eastern Mediterranean region stands out as it has a complex and diverse, but as yet largely unexplored record of volcanic eruptions. Here we present the first distal tephra record for the Eastern Mediterranean region spanning from 335 to 235 ka (corresponding to Marine Isotope Stages [MIS] 9 to 7e); our record has been derived from peat cores from the iconic terrestrial climate archive of Tenaghi Philippon (NE Greece). We have identified twenty-seven cryptotephra layers that represent eruptions from diverse Mediterranean sources. Six cryptotephra layers can be linked to Campanian volcanoes, and another six layers are tentatively correlated to Aeolian Arc volcanism. Of the ten cryptotephra layers that we have identified as deriving from the Aegean Arc, eight originate from Santorini volcano and two are tentatively attributed to either Kos or Milos. Five cryptotephra layers have yet unknown origins.

Most of the identified cryptotephras represent previously undocumented eruptions. We provide age estimates for all cryptotephras and, by extension, for the underlying eruptions based on orbitally tuned pollen data from the same cores. The only cryptotephra layer in the 335–235 ka record from Tenaghi Philippon that represents a previously known eruption has a palynostratigraphically derived age of c. 289 ka and can be tentatively linked to the Seiano Ignimbrite from the Campanian Volcanic Zone; this represents the first time that this eruption can be traced beyond its proximal area. The documentation and geochemical characterization of tephra layers from different Mediterranean sources in the Tenaghi Philippon peat cores for MIS 9–7e is an important step towards the integration of regional Mediterranean tephrostratigraphic information for the Middle Pleistocene.

1 Introduction

Tephrochronology has emerged as a valuable, widely used technique in Quaternary geology because it enables the precise correlation and dating of sedimentary archives using tephra isochrons (Lowe, 2011). Over the recent past, the tracing of volcanic ash layers in distal (>100 km) and ultra-distal (>1000 km) settings with regard to their eruption centers has benefitted from new techniques of glass-shard extraction and single-glass geochemical analyses (e.g., Blockley et al., 2005; Lowe, 2011; Davies, 2015); this has allowed to greatly expand the geographical scale of tephrochronological applications (e.g., Lane et al., 2013; Jensen et al., 2014). The study of distal tephras including macroscopically non-visible tephras, so-called cryptotephras, can be instrumental in assessing the volumes, magnitudes and frequencies of both known and yet undocumented volcanic eruptions (e.g., Sulpizio et al., 2014; Ponomareva et al., 2015; Crocitti et al., in press); these aspects are crucial for predicting the societal and economic hazards and risks of volcanic eruptions (e.g., Bourne et al., 2016; Sandri et al., 2016).

In this context, the Eastern Mediterranean region with its highly explosive Paleogene–Quaternary volcanism merits special attention. The paleoenvironmental and paleoclimatic research in this region requires tephrochronological data in order to date and correlate sedimentary archives (e.g., Leicher et al., 2016; Kousis et al., 2018; Wulf et al., 2018). Moreover, considering that distal tephra records often document yet under-reported eruptions (e.g., Albert et al., 2017), incorporation of such data can help improve volcanic risk assessments for this densely populated region.

To date, a considerable number of studies has been devoted to the establishment of proximal-distal and distal-distal tephra correlations in the Eastern Mediterranean region. They have yielded a relatively advanced tephrostratigraphic framework for the Holocene and Late Pleistocene (e.g., Keller et al., 1978; Aksu et al., 2008; Zanchetta et al., 2011;

Wulf et al., 2018). However, the proximal record of volcanic eruptions in the Mediterranean region becomes increasingly fragmentary when going backwards in time (e.g., Wulf et al., 2012), and only very few studies have yet been carried out on distal tephras from that region that extend beyond the past c. 200 ka (Leicher et al., 2016; Kousis et al., 2018; Vakhrameeva et al., 2018). As a consequence, the regional Italian and Eastern Mediterranean (i.e., Aegean Arc, Anatolia) tephrostratigraphies for the Middle Pleistocene have remained not only rather incomplete, but also largely disconnected (Vakhrameeva et al., 2018).

In light of these limitations, there is clearly a need for archives that preserve distal tephra layers from different source regions. They can play a key role in establishing an integrated volcanic history of the Eastern Mediterranean region that extends beyond the last interglacial. Such an archive is represented by the early to late Pleistocene sediment record from Tenaghi Philippon (NE Greece; Fig. 1). Owing to its unique, peat-dominated lithology, this archive has yielded abundant (crypto)tephra marker horizons within the MIS 5–1 interval (St. Seymour et al., 2004; Lowe et al., 2012; Albert et al., 2015; Pross et al., 2015; Wulf et al., 2018). A recently published cryptotephra record for the MIS 12–10 section of the Tenaghi Philippon archive (Vakhrameeva et al., 2018) forms an important step towards extending Eastern Mediterranean tephrostratigraphy into the Middle Pleistocene. Building upon these studies, we here present cryptotephra data for the upper Middle Pleistocene interval of the Tenaghi Philippon archive spanning from MIS 9 to 7e (335–235 ka).

2 Study site

The Philippi peatland, mostly referred to as "Tenaghi Philippon", is a 55 km^2 large sub-basin in the southeastern part of the Drama Basin, an intermontane tectonic basin in NE Greece (Fig. 1). From the early Pleistocene onwards, limnic and notably telmatic conditions prevailed across most of the Philippi peatland, resulting in a nearly 200 m thick succession that consists predominantly of fen peat (Christanis et al., 1998). Based on palynological information from early drillcores, this succession spans the past ~1.35 Ma continuously (Wijmstra and Smit, 1976; Van der Wiel and Wijmstra, 1987a, b; Tzedakis et al., 2006). Due to its unique lithology, length and stratigraphic completeness, Tenaghi Philippon has emerged as a unique paleoclimate archive for the Quaternary in Europe since its discovery in the 1960s (e.g., Wijmstra, 1969; Wijmstra and Groenhart, 1983; Tzedakis et al., 2006; Pross et al., 2009; see Pross et al., 2015, for an in-depth review). Because the original material from coring campaigns in the 1960s had long deteriorated and was partially also compromised by drilling-related core loss, new, high-quality drillcores were recovered from the Philippi peatland in 2005 and 2009 (Pross et al., 2007, 2015). These cores provided the material for this study.

Geographically, Tenaghi Philippon is located within the potential ash-dispersal areas of a number of volcanic provinces, which – together with its exceptional stratigraphic length and completeness as well as its peat-dominated lithology – makes it a key (crypto)tephrostratigraphic archive for the Eastern Mediterranean region. Considering their proximity to Tenaghi Philippon, the most likely tephra sources during the Middle Pleistocene were the volcanic centers of Italy (Peccerillo, 2017) and the Aegean Arc (Pe-Piper and Piper, 2002) (Fig. 1). Further volcanic provinces that were active during the Middle Pleistocene and may have dispersed tephra particles to Tenaghi Philippon are western (e.g., Platevoet et al., 2014), central (e.g., Şen et al., 2003) and eastern (e.g., Sumita and Schmincke, 2013b) Anatolia, the eastern Carpathians (e.g., Molnár et al., 2018), and the French Massif Central (e.g., Nomade et al., 2012). The potential of Tenaghi Philippon with regard to recording eruptive events produced by various Mediterranean volcanic provinces is supported by the identification of cryptotephras of Italian, Aegean Arc and yet unknown eruptive centers of the Eastern Mediterranean during MIS 5–1 (130–0 ka; Wulf et al., 2018) and MIS 12–10 (460–335 ka; Vakhrameeva et al., 2018).

3 Material and methods

3.1 Core material

Core material from two drilling campaigns in the Philippi peatland was studied for the present paper. The cores TP-2005 (coordinates: 40° 58’ 24.0” N, 24° 13’ 25.2” E; 42 m above sea level) and TP-2009 (40° 57’ 39.5” N, 24° 16’ 03.1” E; 42 m above sea level) were drilled in a distance of 4.4 km from each other in 2005 and 2009, respectively (for details see Pross et al., 2007, 2015). Whereas core TP-2005 comprises the depth interval from 60 to 0 m, core TP-2009 spans the interval from 200 to 50 m depth. For the present study, we have analyzed the core sections from the 60–50 m depth interval of core TP-2005 and the 63–50 m depth interval of core TP-2009 for cryptotephras. Special emphasis was on the identification of cryptotephra layers that occur in both cores. Such a cryptotephra-based correlation of both archives allows critical assessment of correlations derived from palynological and X-ray fluorescence (XRF) core-scanning information (Fig. 2). Lithologically, the studied interval of core TP-2005 consists entirely of peat, whereas the studied interval of core TP-2009 consists of peaty mud and lake marls (63–58.5 m) and peat (58.5–50 m; compare Fig. 2).

3.2 Cryptotephra analysis

3.2.1 Extraction of glass shards

In a first analytical step, the cores were explored for cryptotephra layers using 10-cm-long contiguous sub-samples. Subsequently, the intervals that had yielded glass shards were investigated in 1 cm resolution in order to determine the exact stratigraphic position of cryptotephras. The extraction of glass shards from the host sediment and their preparation for geochemical analysis were carried out using commonly applied techniques (compare Vakhrameeva et al., 2018, for an in-depth description of the processing protocol). The identified cryptotephras were labeled according to the scheme previously introduced for Tenaghi Philippon cores (Wulf et al., 2018), with the abbreviation of the coring campaign (TP05 or TP09) being followed by the mid-point of the sample-depth range (in meters) where a cryptotephra was detected (e.g., cryptotephra TP09-55.35).

3.2.2 Geochemical analysis of glass shards

3.2.2.1 Electron probe microanalysis (EPMA)

Major-element analysis of single glass shards was performed using a wavelength-dispersive (WDS) electron microprobe JEOL JXA-8500F at the German Research Centre for Geosciences in Potsdam. The analytical conditions included an accelerating voltage of 15 kV, a 10 nA beam current, and a 3–10 µm beam with count times of 20 s for the elements Mg, P, Cl, Ti, Mn, and Fe, and 10 s for F, Ca, Al, Si, K, and Na (analyzed first). MPI-DING reference glasses such as GOR128-G, GOR132-G, ATHO-G and StHs6/80 (Jochum et al., 2006) as well as natural Lipari obsidian (Hunt and Hill, 1996; Kuehn et al., 2011) served as secondary glass standards and were measured once prior to sample analyses to ensure inter-laboratory consistency of analytical data (Supplement 1). The EPMA results were normalized to 100% total oxides on a volatile-free basis to facilitate data comparison. Low values of total oxides (i.e., <90% for rhyolitic and <95% for other glass shards) were excluded from the dataset, apart from two tephras for which no better-quality analyses could be obtained.

3.2.2.2 Secondary Ion Mass Spectrometry (SIMS)

Selected glass shards were analyzed for trace elements using a CAMECA ims3f ion probe at the Institute of Earth Sciences, Heidelberg University, using a 14.5 keV, ~10 nA $^{16}O^{-}$ primary ion beam with a spot diameter of ~15 µm. Positive secondary ions were accelerated to 4.5 keV, and the energy filter was set to accept ions with a starting energy of 105±25 eV. The imaged field of the secondary ion optics was limited to a diameter of ~13 µm (nominal imaged field 25 µm, 400 µm field aperture), and the mass resolving power was ~400 (at 10% intensity). The setup used a pre-sputtering time of 270 s (including calibration of all peak positions prior to each analysis) and five acquisition cycles with integration times of 2 s (^{30}Si), 5 s (^{85}Rb, ^{88}Sr, ^{89}Y, ^{90}Zr, ^{93}Nb, ^{138}Ba, ^{139}La, ^{140}Ce) and 20 s (^{232}Th, ^{238}U) per cycle. The NIST SRM 610 glass standard was employed as an internal standard (concentrations taken from Jochum et al., 2011), and the ATHO-G, StHs6/80-G, and GOR132-G glasses (Jochum et al., 2006) were used as secondary reference materials (Supplement 1).

3.3 XRF core scanning

The elemental composition of the TP-2005 and TP-2009 cores was determined semi-quantitatively with a 4th generation Avaatech XRF core scanner at the Institute of Earth Sciences, Heidelberg University. The fresh and smooth split core surface was covered with Ultalene prior to scanning to avoid contamination of the XRF detector and desiccation of the core. Measurements were acquired every 5 mm with a rhodium X-ray source (10 kV, 200 mA, 10 s) to cover the elements Al, Si, S, K, Ca, Ti, Mn, and Fe. To minimize the sample geometry effects (e.g., water content, surface irregularities, sediment density), element intensities (cps) were normalized by center-log-ratio (CLR) transformation (Weltje et al., 2015).

3.4 Pollen analysis

Based on the notion that the tree-pollen percentages at Tenaghi Philippon closely mirror glacial/interglacial cycles (e.g., Mommersteeg et al., 1995; Tzedakis et al., 2006; Milner et al., 2016), tree-pollen percentages were used to obtain pollen-based age constraints for the cryptotephra layers identified in the succession. For the examined interval of the TP-2005 core, the high-resolution (sample distance: 4 cm, equivalent to a mean temporal resolution of ~290 years) pollen dataset of Fletcher et al. (2013) was used. For core TP-2009, the available low-resolution pollen dataset of Pross et al. (2015) was augmented by an additional 22 new pollen samples covering the MIS 9e–d interval at a spacing of 18 cm (mean temporal resolution: ~1140 years). Palynological processing followed standard techniques that are described in detail in Fletcher et al. (2013) and Pross et al. (2015). The calculation of tree-pollen percentages was based on counting sums of at least 300 pollen grains excluding Poaceae, Cyperaceae, aquatic plants, and fern spores.

4 Core alignment and age model

Previous low-resolution pollen analysis has suggested that the 60–50 m interval of core TP-2005 broadly overlaps with the 60–50 m interval of core TP-2009 (Pross et al., 2015). Temporally, this overlap corresponds to MIS 9c–7e (c. 312–235 ka; Fletcher et al., 2013). The new element records for the respective intervals of the TP-2005 and TP-2009 cores derived from XRF scanning allow substantial refinement of the correlation between the cores. Specifically, variations in normalized Si_{CLR} records show a distinct pattern that enabled unambiguous alignment and, together with the available palynostratigraphic information, reliable age control for both cores (Figs. 2 and S1). At Tenaghi Philippon, the element Si is predominantly an indicator for detrital material with relatively higher amounts during cold stages (Kalaitzidis and Christanis, 2002; Kalaitzidis, 2007). Although the Philippi peatland represents a minerotrophic rather than an ombrotrophic setting, two independent lines of evidence suggest that Si has reached the peatland primarily through aeolian rather than aquatic transport. Firstly, the core sections examined in our study are predominantly composed of peat and (to a lesser extent) of lake marls (Fig. 2), with no lithological indication that would suggest fluvially influenced sedimentation (Fig. 2). Secondly, the Si curve matches well with the percentages of steppe-element pollen at Tenaghi Philippon (Fig. S2). Steppe elements dominated the catchment area during cold and dry phases when aeolian dust dominated the supply of detrital matter, and their percentages were lowest during warmer, more humid intervals (Pross et al., 2009; Müller et al., 2011; Fletcher et al., 2013). Hence, the relative amount of Si was maximal under the driest and coldest conditions when aeolian dust dominated.

The Si-based core alignment did not only allow us to refine the overlap interval to 60 to 50.62 m, but also revealed an offset in the age/depth relationships of the TP-2005 and TP-2009 cores. This offset generally increases from the top (0.62 m) to the bottom (1.35 m) of the overlap interval. Based on the high-resolution palynostratigraphic age control for core TP-2005, the sediment at the top of the TP-2005 core segment at 50.44 m depth is 4.98 ka younger than in the TP-2009 core segment of the same depth; at the bottom (i.e., at 58.45 m) the age difference amounts to 7.94 ka (Table S1). These variations in offset across the overlap interval can be primarily attributed to changes in sedimentation rates and/or post-depositional compaction; to a lesser extent, they may also result from drilling-related processes such as non-uniform expansion of the peat in the drill cores depending on slight differences in lithology and water content. When calibrated against the time domain, the refined overlapping interval is from c. 312 to 240 ka. This Si-based correlation allows the integration of pollen datasets from cores TP-2005 and TP-2009 (Fig. 3).

To establish a chronology for the studied core sections, the previously published age model of Fletcher et al. (2013) for the 60–50 m depth interval of core TP-2005 was integrated with a newly developed age model for the 82–63 m depth interval of core TP-

2009 (Vakhrameeva et al., 2018). Specifically, the pollen data from Fletcher et al. (2013) were aligned to the Iberian margin MD01-2443 sea-surface temperature (Martrat et al., 2007) and pollen (Roucoux et al., 2006) record. Since the latter was aligned via benthic oxygen isotope values ($\delta^{18}O_{benthic}$) to the EPICA Dome C (EDC) Antarctic temperature record, this allowed placing the TP-2005 pollen data on the Antarctic ice core timescale EDC3 (Parrenin et al., 2007). The pollen dataset newly generated for the present paper for the 63–59 m depth interval of core TP-2009 was aligned to that from a previously recovered core from Tenaghi Philippon (TF-II; Wijmstra and Smit, 1976) using the orbitally tuned age model of Tzedakis et al. (2006), thereby following the procedure given in Vakhrameeva et al. (2018) (see Table S2 for details).

The chronological uncertainties that arise from using different approaches in the development of age models for the TP-2005 and TP-2009 cores are within the uncertainties inherent in the age models used. The error in the EDC3 timescale for the studied interval amounts to 6 ka (Parrenin et al., 2007), and an additional uncertainty of ~0.3 ka is introduced through the correlation of the MD01-2443 $\delta^{18}O_{benthic}$ and TP-2005 pollen records (Fletcher et al., 2013). Nevertheless, the palynologically derived age estimates for cryptotephras provided in our study are precise enough to facilitate distal tephra correlations.

5 Results

5.1 Cryptotephra record

The Tenaghi Philippon cryptotephra record for the MIS 9–7e interval comprises 29 cryptotephra layers, of which 22 cryptotephras were identified in core TP-2009 and 7 cryptotephras were extracted from core TP-2005 (Table 1). The core alignment via XRF-scanning-derived Si data allowed to resolve the stratigraphic relationship between cryptotephra layers found in both cores (Fig. 3). A total of 25 cryptotephra layers were detected within the MIS 9 interval (c. 324–289 ka), whereas only 4 cryptotephra layers were detected in the MIS 7 interval (c. 240–235 ka). Glass-shard concentrations in the cryptotephra samples range from 0.2 to 24 shards per gram dry weight (shards/g_{dwt}). All cryptotephra layers were characterized by EPMA, and ten cryptotephra layers contained shards that were large enough to be analyzed by SIMS. It is noteworthy that several of the obtained isochrons are based on currently limited geochemical information; in addition, some shards yielded only low analytical totals (<95%); however, even limited geochemical data can still provide an indication of their source, as it has been demonstrated by previously reported cryptotephra layers from Tenaghi Philippon with similarly low numbers of shards analyzed (Wulf et al., 2018). Representative EPMA and SIMS glass data (single analytical points) are given in Table 2, and full analytical data can be found in Supplement 1. Figure 4 shows normalized (volatile-free) EPMA data as plotted on the total alkali *vs*. silica (TAS) classification diagram (Le Bas et al., 1986). Beyond the cryptotephra layers mentioned above, five cryptotephra levels have been detected in core TP-2009 (Table 1); however, extraction of glass shards from these levels for geochemical analysis was precluded by the low concentrations, small sizes and vesicular nature of the shards in these samples. In the following, the identified cryptotephra layers are described in ascending stratigraphic order for the TP-2009 and TP-2005 cores.

5.1.1 Cryptotephra layers TP09-61.35 to TP09-60.25 (7 layers, c. 324–318 ka)

Three cryptotephra layers (TP09-61.35, TP09-60.935, and TP09-60.85) are located within an interval characterized by very high (>90%) tree-pollen percentages, implying that they were deposited during the warmest part of MIS 9 (i.e., MIS 9e; Railsback et al., 2015) between 324 and 320 ka (Fig. 3). Four younger cryptotephra layers (TP09-60.65, TP09-60.35, TP09-60.335, and TP09-60.25) occur within an interval with decreasing (86–

32%) tree-pollen percentages corresponding to the first cooling phase within MIS 9 (i.e., MIS 9d; Railsback et al., 2015). Based on palynostratigraphic age control, they can be assigned ages of c. 319 and 318 ka.

Five of these cryptotephra layers (i.e., TP09-61.35, -60.935, -60.85, -60.65, and -60.25) with very low glass-shard concentrations of 0.4 to 4 shards/g_{dwt} (Table 1) are rhyolites (70.0–72.2 wt% SiO_2; alkali ratios of 0.64–0.79; normalized data) that straddle the boundary between medium and high K_2O concentrations (2.9–3.3 wt%) (Table 2; Fig. 4a, b, c). They are generally very similar in their major-element composition, except for one apparently low Na_2O value (1.2 wt%) shown by cryptotephra layer TP09-60.25 that is likely due to Na loss during EPMA (Table 2).

The range-finder and high-resolution samples TP09-60.35 and TP09-60.335 with glass-shard concentrations of 1 and 4 shards/g_{dwt}, respectively, show distinct major-element chemistries. Cryptotephra layer TP09-60.35 classifies as a high-K calcalkaline rhyolite with concentrations of 73.7 wt% SiO_2, 4.4 wt% K_2O, 1.7 wt% Na_2O, and 3.4 wt% MgO, and an alkali ratio of 2.68 (Table 2; Fig. 4a, b, c). The trace-element data indicate a pronounced depletion in concentrations of high field strength elements (HFSE), in particular Nb, Zr, Th, and U as well as rare earth elements (REE, i.e., Y, La, Ce), and elevated abundances of large ion lithophile elements (LILE, i.e., Ba, Rb, Sr; Table 2; Figs. 4d and S3). Cryptotephra layer TP09-60.335 is a calcalkaline dacitic tephra characterized by 64.5 wt% SiO_2, 2.0 wt% K_2O, 4.5 wt% Na_2O, and an alkali ratio of 0.43 (Table 2; Fig. 4).

5.1.2 Cryptotephra layers TP09-60.055a, -60.055b, -60.05a, and -60.05b (2 layers, c. 317 ka)

Four cryptotephra components were identified in the TP-2009 sample at 60.0–60.1 m core depth. The pollen record in this interval is characterized by a sharp decrease from high (86%) to relatively low tree-pollen percentages (32%), corresponding to the first cooling phase within MIS 9 (i.e., MIS 9d; Railsback et al., 2015; Fig. 3).

The low-resolution tephra scan of sample TP09-60.05 revealed two trachytic and two rhyolitic components with a total glass-shard concentration of 14 shards/g_{dwt}. Two distinct trachytic compositions labeled TP09-60.05a and TP09-60.05b could not be replicated during the high-resolution (1-cm) tephra scan; therefore, their stratigraphic position could not be further refined. The first trachytic cryptotephra component TP09-60.05a (1 analysis) is characterized by 61.3 wt% SiO_2, 9.2 wt% K_2O, 3.3 wt% Na_2O, 2.6 wt% CaO, 0.80 wt% MgO, and 0.35 wt% Cl (Table 2; Fig. 4a). The alkali ratio of 2.77 assigns it to ultra-potassic rocks (Fig. 4c). The second trachytic component TP09-60.05b (seven analytical points) has slightly higher SiO_2 concentrations (62.1–63.1 wt%) but lower alkali ratios (1.05–1.32) as they are indicative of shoshonites (Fig. 4a, c). It can be further distinguished from TP09-60.05a by lower CaO and MgO contents (1.2–1.8 and 0.32–0.39 wt%, respectively) as well as higher Cl values (0.72–0.90 wt%) (Table 2). Differences between the two trachytic components also emerge from the SIMS trace-element dataset showing that component TP09-60.05b is more enriched in HFSE (including REE) and depleted in some of LILE (Sr, Ba) compared to TP09-60.05a (Table 2; Figs. 4d and S3).

The high-resolution tephra scan of the 60.0–60.1 m interval revealed an additional cryptotephra level at 60.055 m depth (6 shards/g_{dwt}), which contained two distinct rhyolitic compositions, here labeled as TP09-60.055a and TP09-60.055b. These compositions are identical to those found in sample TP09-60.05. Cryptotephra component TP09-60.055a (four analyses) exhibits SiO_2 concentrations of 69.9–73.9 wt% and a calcalkaline to high-K calcalkaline affinity (3.1–4.5 wt% K_2O, 3.4–4.8 wt% Na_2O; Fig. 4a, b, c). The trace-element dataset is defined by enrichment in LILE relative to HFSE including REE (Table 2; Figs. 4d and S3). Cryptotephra component TP09-60.055b (three shards) is a high-silica rhyolite (76.6–77.7 wt% SiO_2) with high-K calcalkaline affinity (4.8–5.0 wt%

K_2O, 2.4–3.4 wt% Na_2O; Fig. 4a, b, c). The trace-element composition is similar to that of cryptotephra component TP09-60.055a, except for slightly lower Zr/LILE ratios (Table 2; Figs. 4d and S3).

5.1.3 Cryptotephra layers TP09-59.995, -59.95a, -59.95b, and -59.935 (4 layers, c. 317–316 ka)

Four distinct cryptotephra components were detected in the TP-2009 core at 59.9–60.0 m depth, during the first cooling phase within MIS 9 (i.e., MIS 9d; Railsback et al., 2015; Fig. 3). One trachytic (TP09-59.95a) and one rhyolitic (TP09-59.95b) cryptotephra component with a total glass-shard count of 1 shard/g_{dwt} were identified in the low-resolution tephra sample at c. 316 ka. The major-element composition of the trachytic glass component TP09-59.95a is defined by 62.2 wt% SiO_2 and an alkali ratio of 1.77, which classifies it as a potassium-rich trachyte (Fig. 4a, c). It is further characterized by values of 1.7 wt% CaO, 0.79 wt% MgO, and 0.37 wt% Cl (Table 2). The trace-element concentrations display high LILE/HFSE and LILE/REE ratios (Table 2; Figs. 4d and S3). Cryptotephra component TP09-59.95b is a high-K calcalkaline high-silica rhyolite (76.7 wt% SiO_2) with K_2O and Na_2O values of 4.7 wt% and 3.0 wt%, respectively (Table 2; Fig. 4a, b, c).

The high-resolution sample scan of the 59.9–60.0 m interval revealed two additional cryptotephra horizons, TP09-59.995 and TP09-59.935. These are, however, geochemically distinct from the above-mentioned rhyolitic composition. They have low glass-shard counts of 2 and 3 shards/g_{dwt} and are dated palynostratigraphically to 317 and 316 ka, respectively. Both cryptotephra layers show similar major-element characteristics with concentrations of 71.8–73.4 wt% SiO_2, 4.1–4.5 wt% K_2O and low Na_2O values (1.1–1.5 wt%) suggesting a classification as high-K calcalkaline rhyolites (Fig. 4a, b, c). The main compositional differences are their MgO (2.4 wt% in TP09-59.935

vs. 3.6 wt% in TP09-59.995) and Al_2O_3 concentrations (15.6–16.2 wt% *vs.* 14.2 wt%, respectively) (Table 2).

5.1.4 Cryptotephra layers TP09-59.85 and -59.45 (2 layers, c. 316–314 ka)

Cryptotephra layers TP09-59.85 and TP09-59.45 have glass-shard counts of 0.2 and 1 shards/g_{dwt}. They occur within an interval of increasing (64–90%) tree-pollen percentages at the onset of the first warm phase within the later part of MIS 9 (i.e., MIS 9c; Railsback et al., 2015; Fig. 3). Their positions within the TP-2009 core yield age estimates of c. 316 and 314 ka, respectively.

Both layers represent rhyolites, albeit with slightly different major-element compositions. TP09-59.85 is characterized by concentrations of 76.2 wt% SiO_2, 1.0 wt% Na_2O, and 3.6 wt% K_2O (Fig. 4a, b, c). TP09-59.45 is less silicic (74.5 wt% SiO_2), richer in alkalis (1.5 wt% Na_2O and 4.7 wt% K_2O), and differs in higher FeO (1.4 wt% *vs.* 1.0 wt% in TP09-59.85) and lower CaO values (1.2 wt% *vs.* 2.1 wt% in TP09-59.85) (Table 2; Fig. 4a, b, c). Its trace-element spectrum is defined by very low concentrations of HFSE and REE, and relatively high concentrations of LILE (Table 2; Figs. 4d and S3).

5.1.5 Cryptotephra layers TP09-59.245 and -59.235 (2 layers, c. 313 ka)

A rhyolitic cryptotephra layer was detected in the low-resolution sample TP09-59.25 and subsequently replicated in the high-resolution sample TP09-59.245 yielding a glass-shard concentration of 2 shards/g_{dwt}. Another trachytic cryptotephra component with a glass-shard count of 3 shards/g_{dwt} was extracted from the contiguous high-resolution sample TP09-59.235. Both cryptotephra layers are from a core interval with high (72–85%) tree-pollen percentages during the first warm phase within the later part of MIS 9 (i.e., MIS 9c; Railsback et al., 2015; Fig. 3). They have a palynologically derived age of c. 313 ka.

The major-element composition of the rhyolitic cryptotephra layer TP09-59.245 indicates relatively low SiO_2 concentrations (69.7–70.7 wt%) with medium to high values of K_2O (2.9–3.5 wt%; Fig. 4a, b). The Na_2O concentrations (4.7–4.9 wt%) are higher than those of K_2O, and the alkali ratios are 0.60–0.74 (Fig. 4c). The SIMS trace-element data document depleted HFSE and REE concentrations in relation to the elevated abundances of LILE (Table 2; Figs. 4d and S3).

Cryptotephra layer TP09-59.235 has 62.0 wt% SiO_2, Na_2O (7.3 wt%) exceeding K_2O values (5.0 wt%), and an alkali ratio of 0.68 defining it as a sodium-rich trachyte (Fig. 4a, c). Its composition is further characterized by concentrations of 1.5 wt% CaO, 0.59 wt% MgO, and 0.45 % Cl, and trace-element data that show a moderate enrichment in LILE relative to Nb, Zr and REE (Table 2; Figs. 4d and S3).

5.1.6 Cryptotephra layers TP09-55.35, -55.095, and -55.045 (3 layers, c. 290–289 ka)

The rhyolitic cryptotephra layer TP09-55.35 with a glass-shard count of 1 shard/g_{dwt} and the chemically distinct K-alkaline cryptotephra layers TP09-55.095 and TP09-55.045 (with glass-shard counts of 2 shard/g_{dwt}, respectively) occur in an interval of high (60–94%) tree-pollen percentages that characterize the second warm phase within the later part of MIS 9 (i.e., MIS 9a; Fletcher et al., 2013; Railsback et al., 2015; Fig. 3). This allows their ages to be constrained to c. 290 ka (TP09-55.35) and 289 ka (TP09-55.095, TP09-55.045).

Cryptotephra layer TP09-55.35 has major-element concentrations of 73.1–73.8 wt% SiO_2, 4.8–5.2 wt% K_2O, 1.6–2.2 wt% Na_2O, and 1.8–2.2 wt% MgO, which define it as a high-K calcalkaline rhyolite (Fig. 4a, b and c). The shards are enriched in LILE, while HFSE and REE are depleted (Table 2; Figs. 4d and S3).

Cryptotephra layers TP09-55.095 and TP09-55.045 are two closely spaced layers that are distinguishable on the basis of their major-element characteristics. TP09-55.095 (1 analysis) classifies as a potassium-rich trachyandesite with values of 57.2 wt% SiO_2, 5.7 wt% FeO, 4.4 wt% CaO, 3.2 Na_2O, and 7.8 wt% K_2O (Table 2; Fig. 4a, c). The younger TP09-55.045 cryptotephra layer (1 analysis) is a potassium-rich trachyte with higher SiO_2 concentrations (63.5 wt%), lower FeO (2.5 wt%) and CaO values (2.0 wt%), and Na_2O and K_2O levels of 4.5 wt % and 7.6 wt%, respectively (Table 2; Fig. 4a, c). Concentrations of Cl are comparable in both cryptotephra layers (0.54 wt% in TP09-55.095 and 0.66 wt% in TP09-55.045).

5.1.7 Cryptotephra layers TP05-56.475, -56.45, and -56.41 (3 layers, c. 289 ka)

The oldest cryptotephra layers in the examined part of core TP-2005 are situated at a depth of 56.4–56.5 m. They occur during the second warm phase within the later part of MIS 9 as defined by high (60–94%) tree-pollen percentages (i.e., MIS 9a; Fletcher et al., 2013; Railsback et al., 2015; Fig. 3) and can be assigned an age of c. 289 ka.

A rhyolitic cryptotephra layer with a glass-shard count of 1 shard/g_{dwt} was identified in the low-resolution sample TP05-56.45. Subsequently, two additional layers of similar trachyphonolitic to trachytic composition were identified in the high-resolution samples TP05-56.475 and TP05-56.41, yielding glass-shard concentrations of 10 and 7 shards/g_{dwt}, respectively.

The rhyolitic cryptotephra TP05-56.45 has a high-silica composition (75.6–75.9 wt% SiO_2). With K_2O values of 3.3–3.4 wt% it straddles the boundary between the calcalkaline and high-K calcalkaline fields (Fig. 4a, b). It shows low Na_2O contents (1.5 wt%) as well as relatively high MgO values (1.7 wt%) (Table 2; Fig. 4c). The major-element composition of cryptotephra layer TP05-56.45 resembles that of the above described cryptotephra layer TP09-55.35 from core TP-2009, except for significantly lower FeO and K_2O concentrations (0.5–0.6 wt% *vs.* 1.2–1.5 wt% and 3.3–3.4 wt% *vs.* 4.8–5.2 wt%, respectively), and higher CaO concentrations (3.1–3.3 wt% *vs.* 1.1–1.3 wt% in TP09-55.35) (Table 2).

Three analytical data points have been obtained for cryptotephra layer TP05-56.475, defining it as a trachyte that straddles the phonolitic boundary (Fig. 4a). The major-element chemistry is characterized by concentration ranges of 58.7–59.3 wt% SiO_2, 4.1–4.6 wt% FeO, 3.4–3.6 wt% CaO, 3.6–3.8 wt% Na_2O, and 8.4–8.7 wt% K_2O (Table 2). The alkali ratio of 2.20–2.41 defines this tephra as potassic (Fig. 4c). In comparison, cryptotephra layer TP05-56.41 (5 analyses) has a less homogenous and slightly more evolved composition (59.1–63.1 wt% SiO_2; Fig. 4a). Slightly elevated Na_2O and K_2O concentrations of 3.6–4.2 wt% and 8.4–9.6 wt% and the resulting high alkali ratios of 2.07–2.70 indicate a potassic to ultra-potassic composition (Fig. 4c) that also differs from TP05-56.475 by lower FeO (2.8–3.7 wt%) and CaO (2.2–3.2 wt%) values. The Cl concentrations of both cryptotephra layers are comparable, being in the range of 0.44–0.67 wt% (Table 2).

5.1.8 Cryptotephra layers TP05-50.75, -50.55, -50.45, and -50.05 (4 layers, c. 240–235 ka)

The youngest cryptotephra layers in the studied interval derive from low-resolution scanning samples from core TP-2005 between 51 and 50 m depth. This interval is associated with high (>80%) tree-pollen percentages during the oldest part of MIS 7 (i.e., MIS 7e; Fletcher et al., 2013; Railsback et al., 2015; Fig. 3) and dates to c. 240–235 ka. Four cryptotephra levels (TP05-50.75, TP05-50.55, TP05-50.45, and TP05-50.05) have been identified with glass-shard concentrations of 24, 2, 1, and 3 shards/g_{dwt}, respectively. Their major-element data define them as rhyolites with calcalkaline to high-K calcalkaline affinity (Fig. 4a, b). The compositions of all four cryptotephra layers are identical. The relatively wide ranges of concentrations in SiO_2 (71.8–75.9 wt%), MgO

(1.4–3.1 wt%), CaO (2.9–7.0 wt%), Na_2O (0.4–2.6 wt%), and K_2O (2.7–5.0 wt%) reflect high abundances of microcrystal inclusions. FeO values are typically very low (0.2–0.7 wt%; Table 2).

6 Origin of cryptotephras

Cryptotephra layers from the MIS 9–7e interval of the Tenaghi Philippon archive show diverse glass geochemical compositions that range from trachy-phonolites to high-silica rhyolites (Fig. 4). These compositions largely resemble those identified by Vakhrameeva et al. (2018) in the MIS 12–10 interval of the same archive and are therefore grouped into the previously introduced glass geochemical populations POP1 to 5 (Figs. 4–7). They also partly overlap with the trachy-phonolitic and rhyolitic glass compositions documented for the MIS 5 to 1 interval at Tenaghi Philippon, which were almost entirely assigned to known eruptive events (Wulf et al., 2018). In this study, the trachy-phonolitic population POP1, which can be subdivided into three sub-populations (POP1A to POP1C), is derived from Campanian volcanoes (see Section 6.1). The dacitic POP2 and rhyolitic POP3 populations most likely originate from Santorini in the Aegean Arc (Section 6.2). The high-silica rhyolitic POP4 population probably also derives from the Aegean Arc, although Santorini can be excluded as a source (Section 6.3). A newly defined POP6 rhyolitic composition is likely related to Aeolian Arc volcanism (Section 6.4). Finally, another distinct rhyolitic population (POP5) remains undefined with regard to its origin (Section 6.5).

In order to discern primary cryptotephra layers from potentially re-deposited material, we have used several criteria including (i) glass-shard concentration profiles, (ii) geochemical homogeneity/heterogeneity of cryptotephra layers, (iii) previous evidence from tephrostratigraphical analyses at Tenaghi Philippon (Vakhrameeva et al., 2018; Wulf et al., 2018) for the downcore re-deposition of glass shards from visible, thick tephra layers caused by drilling processes. Although the significance of some cryptotephra layers as isochronous markers remains ambiguous at this stage, they nevertheless provide important information for the future identification of new potential key tephra markers in the Eastern Mediterranean region.

6.1 Cryptotephras of Campanian provenance

6.1.1 Cryptotephra layers TP09-60.05a and TP09-60.05b

The oldest Italian cryptotephra layer TP09-60.05 in the studied core interval has a palynologically derived age of c. 317 ka and consists of two trachytic components (POP1A and POP1B). Both components match the major- and trace-element compositions of the basal fall and lower and intermediate flow units (TP09-60.05b) and the upper flow unit (TP09-60.05a) of the Campanian Ignimbrite (CI, 39.85±0.14 ka; Giaccio et al., 2017a) (Figs. 5b, c and S4). The CI is present as a 23-cm-thick layer at 12.87 m in core TP-2005 (Müller et al., 2011); its components are prone to downcore displacement by coring-related processes, primarily affecting the topmost parts in a number of core segments of the TP-2005 core (Wulf et al., 2018). Re-deposited CI material has also been reported from core TP-2009 at 63.015–63.05 m depth (Vakhrameeva et al., 2018). Together with the geochemical evidence, these observations support the interpretation of cryptotephra layer TP09-60.05 to represent re-deposited CI.

6.1.2 Cryptotephra layers TP09-59.95a and TP09-59.235

The trachytic components of cryptotephra layers TP09-59.95a (POP1A) and TP09-59.235 (POP1C) with age estimates of c. 316 and 313 ka, respectively, exhibit relatively low alkali ratios (0.68–1.77; Fig. 5a) and increased Cl concentrations relative to CaO/FeO ratios. This strongly supports a Campanian origin. Specifically, in the CaO/FeO *vs.* Cl discriminative diagram (Giaccio et al., 2017b) the cryptotephras unambiguously plot within the Ischia compositional field (Fig. 5b). They closely match Ischia compositions in other major- and trace-element plots as well (Figs. 5c and S4).

The eruptive history of the island of Ischia dates back to at least 150 ka (e.g., Poli et al., 1987). Ischia is part of the Campanian Volcanic Zone that has been active since the last c. 290 ka (De Vivo et al., 2001; Rolandi et al., 2003), although an even earlier onset of volcanic activity at c. 720 ka is supported by several findings of distal tephras in Middle Pleistocene deposits of the Italian and Balkan Peninsulas (e.g., Giaccio et al., 2013, 2014; Petrosino et al., 2015; Figs. 5c and S4). The recent discovery of a potentially Ischia-derived cryptotephra layer in the MIS 11 interval of the TP-2009 core (TP09-70.45, c. 391 ka; Vakhrameeva et al., 2018; Figs. 5 and S4) suggests that an Ischia/Campanian source for cryptotephra layers TP09-59.235 and TP09-59.95a is well possible. However, the current lack of evidence for volcanic activity during MIS 9 in the proximal and distal Campanian tephrostratigraphic record precludes detailed correlations of these tephras.

6.1.3 Cryptotephra layers TP09-55.095 and -55.045, and TP05-56.475 and -56.41

These trachyphonolitic cryptotephra layers (POP1A) have relatively high alkali ratios (1.67–2.70) and major-element compositions that overlap with those of Campi Flegrei, Roccamonfina, and Roman volcanoes (Figs. 5a and S4). However, the CI *vs.* CaO/FeO plot (Fig. 5b) clearly attributes all cryptotephra layers to Campanian volcanoes, and in particular to Campi Flegrei activities.

The two trachyphonolitic cryptotephra layers from core TP-2005 (TP05-56.475 and -56.41) only marginally overlap in some major-element plots. However, they show the same evolutionary trend as the Campi Flegrei field (Figs. 5a, c and S4), with cryptotephra layer TP05-56.41 partly overlapping with the upper flow unit of CI and cryptotephra layer TP05-56.475 being less evolved than the CI (Figs. 5c and S4). The trachyandesitic TP09-55.095 and trachytic TP09-55.045 cryptotephra layers from core TP-2009 follow the same trend, being less and more evolved than the TP-2005 cryptotephras, respectively (Figs. 5a, c and S4).

Because the age of the cryptotephra layers is c. 289 ka, whereas the volcanic activity at Campi Flegrei is restricted to c. 60 ka (Pappalardo et al., 1999), we define their provenance as Campanian. The oldest deposits of the Campanian Volcanic Zone are exposed in the western foothills of the Apennine Mountains, where the CI is underlain by a suite of older ignimbrites with $^{40}Ar/^{39}Ar$ sanidine ages between c. 290 and 116 ka (De Vivo et al., 2001; Rolandi et al., 2003). Specifically, the oldest Seiano Ignimbrite is dated to c. 289.6±1.9 ka (lowermost sample VE-2B) and 245.9±3.0 ka (uppermost sample VE-2A), the former date being well consistent with our palynologically derived ages of c. 289 ka for the detected cryptotephra layers. Geochemical analyses of these highly weathered ignimbrites were carried out by Belkin et al. (2016); however, the generated whole-rock data exhibit highly altered major-element compositions that are not suitable for comparison with the Tenaghi Philippon cryptotephra glass data. Pristine major-element glass compositions from the younger Taurano Ignimbrite (c. 157.4 ka; De Vivo et al., 2001) show, however, that the ignimbrite has a trachyphonolitic chemistry (Amato et al., 2018) that is less evolved than the CI (Figs. 5c and S4); based on trace-element data, Belkin et al. (2016) propose it to be similar to the older Seiano Ignimbrite. Together with the compatible ages, this inference supports a tentative correlation of all four cryptotephra layers with the Seiano Ignimbrite. Based on the observation that in both cores the stratigraphically older cryptotephra layers (i.e., TP05-56.475 and TP09-55.095) are less evolved than the stratigraphically younger cryptotephra layers (i.e., TP05-56.41 and TP09-55.045), the two cryptotephra levels may represent different explosive phases of the Seiano eruption with the repose time of ~400 years based on palynostratigraphic age control.

6.2 Cryptotephras of Santorini provenance (TP09-61.35, -60.935, -60.85, -60.65, -60.335, -60.25, -60.055a, and -59.245)

Seven medium- to high-K calcalkaline rhyolitic cryptotephra layers of glass population POP3 (TP09-61.35 to TP09-59.245) and one dacitic calcalkaline cryptotephra layer of glass population POP2 (TP09-60.335) best match Santorini tephra compositions in both major- and trace-element plots (Figs. 6a, 7, S5 and S6). Middle and Late Quaternary activity of Santorini is documented by twelve major and numerous minor pyroclastic units of the Thera Pyroclastic Formation (Druitt et al., 1999). When compared to other volcanoes of the South Aegean Arc, Santorini is characterized by generally less evolved tephra compositions (Druitt et al., 1999).

All cryptotephra layers are closely spaced, with the ages of the rhyolitic cryptotephras ranging between 324 and 313 ka and the age of the dacitic layer being c. 318 ka. In the Santorini tephrostratigraphy, this timing corresponds to the interval between the Cape Therma 1 (CTM-1) and Cape Therma 2 (CTM-2) pyroclastic deposits with ages of ≤360 ka and c. 224 ka, respectively, based on K-Ar dating of underlying and overlying lavas (Druitt et al., 1999). Interplinian explosive activity during that time is represented by the minor pyroclastic unit M2 of Druitt et al. (1999). The first distal equivalent of the CTM-1 eruption was recently discovered at Tenaghi Philippon (TP09-65.95, c. 359 ka; Vakhrameeva et al., 2018). The same study also reported a younger cryptotephra layer (TP09-63.015b, c. 336 ka) that represents a yet unknown Santorini eruption within the M2 unit. Because tephrochronological information on the M2 deposits is still lacking, we have compared the cryptotephra layers reported in this study with recently obtained major-element glass data (Vakhrameeva et al., 2018) from older and younger proximal Santorini units, i.e., CTM-1, CTM-2, and Cape Therma-3 (CTM-3) as well as two M1 pumice-fall deposits below CTM-1 (Figs. 6a and S5).

The compositions of the seven rhyolitic cryptotephras are well constrained and partly fall within the extensively overlapping fields of the M1 and CTM-2 glass compositions. In contrast, the dacitic cryptotephra TP09-60.335 displays a major-element composition resembling that of the CTM-1 and CTM-3 tephras (Figs. 6a and S5). This might be indicative for M2 interplinian activity that produced at least two geochemically distinct tephra deposits between 324 and 313 ka.

6.3 Cryptotephras of undefined Aegean Arc provenance (TP09-60.055b and -59.95b)

Two high-silica rhyolitic cryptotephra layers of glass population POP4 geochemically resemble the compositions of tephra deposits from several volcanic provinces including the Aeolian Islands, eastern Carpathians, Aegean Arc, and central Anatolia (Figs. 7 and S6). Based on the age estimates of c. 317 and 316 ka, they most likely represent one single eruptive event. Since cryptotephra TP09-60.055b is situated within an interval containing other tephra components that are considered reworked, we interpret the younger cryptotephra TP09-59.95b (316 ka) as the likely primary layer. A cryptotephra layer with a very similar geochemical fingerprint was identified in the MIS 10 interval of the Tenaghi Philippon archive at c. 358 ka (TP09-65.835b); this tephra most likely derives from Aegean Arc volcanoes, such as Methana, Milos, or Kos (Vakhrameeva et al., 2018). Explosive activity of these sources during the considered time range is represented by the Chelona Series from the Methana peninsula (c. 380–290 ka; Fytikas et al., 1976; Gaitanakis and Dietrich, 1995; Matsuda et al., 1999), the Trachilas complex of Milos (370±90 ka; Fytikas et al., 1986), and the Kefalos Series of Kos (c. 550 ka, maximum eruption age; Pasteels et al., 1986; Bachmann et al., 2010). The available glass and whole-rock geochemical data for the pyroclastic deposits from Milos and Kos show a close fit with cryptotephra layers TP09-60.055b and TP09-59.95b, but too few compositional data exist for Methana volcanics in order to test any correlation (Figs. 6b and S5). More definite tephra assignments will require more tephrochronological data for the Middle Pleistocene of the Aegean Arc and other Mediterranean volcanic sources.

6.4 Cryptotephras of Aeolian Arc sources (TP09-60.35, -59.995, -59.935, -59.85, -59.45, and -55.35)

Six cryptotephra layers in the MIS 9 interval of the TP-2009 core have a homogenous rhyolitic composition (here defined as glass component POP6) that resembles both the composition of younger Aeolian Arc (specifically Lipari) and eastern Carpathian tephras (Figs. 7 and S6). The trace-element compositions of these cryptotephra layers show strongly depleted HFSE and REE relative to LILE (Figs. 7b and S6), indicating affinity to subduction-related tectonic settings (Figs. 4d and S3). Furthermore, because the depletion in HFSE and enrichment in LILE are more pronounced in active or recent subduction settings than in post-subduction settings (Tomlinson et al., 2015), the source of population POP5 is to be sought among active subduction settings. This suggests an origin of the detected cryptotephra layers from Aeolian Arc volcanoes rather than from the eastern Carpathian region. The distribution of cryptotephra occurrences in the analyzed interval of the TP-2009 core shows two temporal clusters that might relate to two distinct eruptive events. The first narrowly spaced cluster of five layers (TP09-60.35 to TP09-59.45) covers the time interval between 318 and 314 ka. It consists of a proposed primary cryptotephra layer TP09-59.935 (c. 316 ka) with the highest glass-shard counts and lower-concentrated, over- and underlying, likely redeposited layers. The second cluster is formed by the geochemically similar cryptotephra layer TP09-55.35 that is dated at c. 290 ka. However, since tephrostratigraphies of the Aeolian Islands and specifically Lipari volcano are still poorly constrained for the MIS 9 time interval, more detailed correlations are not yet possible.

6.5 Cryptotephras of unknown origin (TP05-56.45, -50.75, -50.55, -50.45, and -50.05)

Five cryptotephra layers from the MIS 9 (TP05-56.45; 289 ka) and MIS 7 interval (TP05-50.75 to TP05-50.05; 240–235 ka) in core TP-2005 exhibit a peculiar heterogeneous rhyolitic glass composition (POP5) that stands out by high and variable CaO (2.9–7.0 wt%), very low FeO (0.15–0.66 wt%), and extremely variable Na_2O concentrations (0.4–2.6 wt%; Figs. 7a and S6). The major-element chemistries of these layers are comparable with previously reported cryptotephra layers from the MIS 12 interval at Tenaghi Philippon (Vakhrameeva et al., 2018; Figs. 7a and S6). To date, neither proximal nor distal tephra deposits have been reported from the Eastern Mediterranean volcanic region with respective geochemical glass composition, hindering the allocation of these cryptotephra layers to specific sources.

7 Tephra-based correlation of TP-2005 and TP-2009 cores

The identification of a cryptotephra layer that most likely represents the Seiano eruption from the Campanian Volcanic Zone (compare Section 6.1.3), provides a first-order tie point for the correlation of the two cores. This cryptotephra layer has an older (samples TP05-56.475 and TP09-55.095) and a younger (samples TP05-56.41 and TP09-55.045) component in both cores, with the components having an age difference of ~400 years based on palynostratigraphic age control. Although we consider both components to represent primary fallout deposits that derived from two different phases of the Seiano eruption, we define the stratigraphic position of the tie point at the level of the older cryptotephra component at c. 289 ka because of its higher glass-shard concentration (Table 1). This cryptotephra tie point provides independent validation of the core correlation as previously carried out via XRF-scanning-derived elemental data (compare Section 4).

Comparison of the sequences of cryptotephra layers identified in the TP-2005 and TP-2009 cores across the overlap interval shows that one cryptotephra layer (i.e., TP05-56.45) has been registered only in core TP-2005, whereas another cryptotephra layer (i.e., TP09-55.35) was only found in core TP-2009. Because the coring sites are located only 4.4 km apart from each other within the same, sharply confined basin, this discrepancy appears at first sight difficult to explain. However, similar observations have previously been made on crypto- and macrotephras from peat bogs (Bergman et al., 2004; Watson et al., 2015) and lakes (Boygle, 1999; Pyne-O'Donnell, 2011). Notably, the distances between the coring sites were in these cases often even smaller than between the TP-2005 and TP-2009 sites, ranging from ~1000 m (Boygle, 1999) to as little as 10 m (Pyne-O'Donnell, 2011); moreover, the cryptotephra shard abundances were much higher (tens to thousands of shards per cm^{-3}) than in the present study (Table 1). Irrespective of these findings, a number of studies has shown that (crypto)tephra layers tend to have an uneven distribution within a basin, often with a high spatial variability of glass-shard concentrations (Pyne-O'Donnell, 2011; Watson et al., 2015) or even being present as discontinuous horizons only (Boygle, 1999; Bergman et al., 2004; Pyne-O'Donnell, 2011). In light of these observations and considering the low glass-shard counts of 1 shard/g_{dwt}, it appears highly plausible that the cryptotephra layers TP05-56.45 and TP09-55.35 were only detected in one of the cores.

Another factor that may have caused a patchy tephra distribution in the Philippi peatland is to be sought in the local meteorological conditions that led to uneven ash deposition from the atmosphere (Watson et al., 2015). In this respect, local rainfall may have played a particularly important role as it can considerably increase the fallout of ash particles within a localized area (Langdon and Barber, 2004). Chemical alteration and post-depositional dissolution of volcanic glass in peatland environments may also affect tephra-shard concentrations (Blockley et al., 2005). Support for such a scenario comes from laboratory experiments; they have suggested that the lifetimes of natural rhyolitic and basaltic shards with radius of 1 mm in soils are on the order of 4500 and 500 years, respectively (Wolff-Boenisch et al., 2004).

8 Conclusions

High-resolution cryptotephra study of the MIS 9 to 7e interval at Tenaghi Philippon yielded 27 cryptotephra layers that potentially constitute primary fallout deposits. Based on their geochemical compositions and palynostratigraphically derived ages, most of these cryptotephra layers could be firmly or at least tentatively assigned to their volcanic/eruptive sources in the Central and Eastern Mediterranean regions.

Six trachyphonolitic cryptotephra layers clearly originate from the Campanian Province in Italy. Remarkably, four of them were deposited c. 289 ka ago and thus match temporally with the oldest ignimbrite exposed in the Campanian Volcanic Zone (i.e., the Seiano Ignimbrite). However, due to the lack of unaltered compositional data for the Seino Ignimbrite, only a tentative correlation is yet possible. Two other trachytic cryptotephra layers at c. 316 and 313 ka indicate yet unreported eruptions of Campanian volcanic centers. Six rhyolitic cryptotephra layers possibly relate to explosive activity of another Italian volcanic province, i.e., the Aeolian Arc and in particular Lipari volcano, although the volcanic history of these sources during that time is still largely unknown. The cryptotephras appear to derive from two eruptive events at c. 316 and 290 ka.

Aegean Arc volcanism is represented by eight rhyolitic and dacitic cryptotephra layers from Santorini volcano. They are likely to record M2 interplinian activities at Santorini with at least two unknown source eruptions between 324 and 313 ka. Two rhyolitic cryptotephra layers that were palynostratigraphically dated at c. 317 and 316 ka most probably resulted from one single eruption, either on Kos or Milos. The provenance of five rhyolitic cryptotephra layers with ages clustered at c. 289 ka and 240–235 ka remains yet unknown.

Our tephrostratigraphic results have yielded the first distal tephra record for the MIS 9–7e interval of the Eastern Mediterranean region. Notably, because the cryptotephra layers identified at Tenaghi Philippon are sourced from both Italy and the Aegean Arc, the tephrostratigraphic lattices of the Central and Eastern Mediterranean regions can now be linked. The fact that a number of the cryptotephra layers from Tenaghi Philippon could not be correlated to volcanic sources, let alone specific eruptions, highlights the need for further study of Mediterranean volcanoes and their activity during the Middle Pleistocene. Further proximal and distal tephra studies that include the in-depth characterization of tephra units via geochemical glass analyses and dating techniques are required in order to establish a complete tephrostratigraphic record for the Eastern Mediterranean region.

Our tephrostratigraphic results also proved instrumental in critically assessing the correlation of core material from the Tenaghi Philippon archive. The occurrence of a cryptotephra layer at c. 289 ka that likely represents the Seiano eruption in both cores studied confirms previously established core correlations based on palynological and XRF core-scanning data.

Acknowledgments

Bjarne Friedrichs, Gonca Gençalioğlu Kuşcu, Biagio Giaccio, Jörg Keller, Niklas Leicher, Fabrizio Marra, Paola Petrosino, and Gianluca Sottili are thanked for discussions. Frederik Allstädt, Monika Doubrawa, Ilse Glass, and Alexander Varychev provided technical assistance. This study received financial support by the Deutsche Forschungsgemeinschaft (DFG) to AK and JP (grants KO4960/3 and PR651/19).

References

1. Aksu, A.E., Jenner, G., Hiscott, R.N., Isler, E.B., 2008. Occurrence, stratigraphy and geochemistry of Late Quaternary tephra layers in the Aegean Sea and the Marmara Sea. Marine Geology 252, 174-192.
2. Albert, P.G., Tomlinson, E.L., Smith, V.C., Di Roberto, A., Todman, A., Rosi, M., Marani, M., Muller, W., Menzies, M.A., 2012. Marine-continental tephra correlations: Volcanic glass geochemistry from the Marsili Basin and the Aeolian Islands, Southern Tyrrhenian Sea, Italy. Journal of Volcanology and Geothermal Research 229–230, 74-94.
3. Albert, P.G., Tomlinson, E.L., Lane, C.S., Wulf, S., Smith, V.C., Coltelli, M., Keller, J., Lo Castro, D., Manning, C.J., Muller, W., Menzies, M.A., 2013. Late glacial explosive activity on Mount Etna: Implications for proximal-distal tephra correlations and the synchronisation of Mediterranean archives. Journal of Volcanology and Geothermal Research 265, 9-26.
4. Albert, P.G., Hardiman, M., Keller, J., Tomlinson, E.L., Smith, V.C., Bourne, A.J., Wulf, S., Zanchetta, G., Sulpizio, R., Müller, U.C., Pross, J., Ottolini, L., Matthews, I.P., Blockley, S.P.E., Menzies, M.A., 2015. Revisiting the Y-3 tephrostratigraphic marker: a new diagnostic glass geochemistry, age estimate, and details on its climatostratigraphical context. Quaternary Science Reviews 118, 105-121.
5. Albert, P.G., Tomlinson, E.L., Smith, V.C., Di Traglia, F., Pistolesi, M., Morris, A., Donato, P., De Rosa, R., Sulpizio, R., Keller, J., Rosi, M., Menzies, M., 2017. Glass geochemistry of pyroclastic deposits from the Aeolian Islands in the last 50 ka: A proximal database for tephrochronology. Journal of Volcanology and Geothermal Research 336, 81-107.
6. Amato, V., Aucelli, P.P.C., Cesarano, M., Filocamo, F., Leone, N., Petrosino, P., Rosskopf, C.M., Valente, E., Casciello, E., Giralt, S., Jicha, B.R., 2018. Geomorphic response to late Quaternary tectonics in the axial portion of the

Southern Apennines (Italy): A case study from the Calore River valley. Earth Surface Processes and Landforms 43, 2463–2480.

7. Bachmann, O., Schoene, B., Schnyder, C., Spikings, R., 2010. The $^{40}Ar/^{39}Ar$ and U/Pb dating of young rhyolites in the Kos-Nisyros volcanic complex, Eastern Aegean Arc, Greece: Age discordance due to excess ^{40}Ar in biotite. Geochemistry, Geophysics, Geosystems 11, Q0AA08.
8. Belkin, H.E., Rolandi, G., Jackson, J.C., Cannatelli, C., Doherty, A.L., Petrosino, P., De Vivo, B., 2016. Mineralogy and geochemistry of the older (>40ka) ignimbrites on the Campanian Plain, southern Italy. Journal of Volcanology and Geothermal Research 323, 1-18.
9. Bergman, J., Wastegård, S., Hammarlund, D., Wohlfarth, B., Roberts, S.J., 2004. Holocene tephra horizons at Klocka Bog, west-central Sweden: aspects of reproducibility in subarctic peat deposits. Journal of Quaternary Science 19, 241-249.
10. Blockley, S.P.E., Pyne-O'Donnell, S.D.F., Lowe, J.J., Matthews, I.P., Stone, A., Pollard, A.M., Turney, C.S.M., Molyneux, E.G., 2005. A new and less destructive laboratory procedure for the physical separation of distal glass tephra shards from sediments. Quaternary Science Reviews 24, 1952-1960.
11. Bourne, A.J., Abbott, P.M., Albert, P.G., Cook, E., Pearce, N.J.G., Ponomareva, V., Svensson, A., Davies, S.M., 2016. Underestimated risks of recurrent long-range ash dispersal from northern Pacific Arc volcanoes. Scientific Reports 6, 29837.
12. Boygle, J., 1999. Variability of tephra in lake and catchment sediments, Svínavatn, Iceland. Global and Planetary Change 21, 129-149.

13. Cantner, K., Carey, S., Nomikou, P., 2014. Integrated volcanologic and petrologic analysis of the 1650AD eruption of Kolumbo submarine volcano, Greece. Journal of Volcanology and Geothermal Research 269, 28-43.
14. Christanis, K., Georgakopoulos, A., Fernández-Turiel, J.L., Bouzinos, A., 1998. Geological factors influencing the concentration of trace elements in the Philippi peatland, eastern Macedonia, Greece. International Journal of Coal Geology 36, 295-313.
15. Crocitti, M., Sulpizio, R., Insinga, D.D., De Rosa, R., Donato, P., Iorio, M., Zanchetta, G., Barca, D., Lubritto, C., 2018. On ash dispersal from moderately explosive volcanic eruptions: Examples from Holocene and Late Pleistocene eruptions of Italian volcanoes. Journal of Volcanology and Geothermal Research, in press.
16. Dalabakis, P., Vougioukalakis, G., 1993. The Kefalos Tuff Ring (W. Kos): depositional mechanisms, vent position and model of the evolution of the eruptive activity. Bulletin of the Geological Society of Greece 28, 259-273 (in Greek).
17. Davies, S.M., 2015. Cryptotephras: the revolution in correlation and precision dating. Journal of Quaternary Science 30, 114-130.
18. De Vivo, B., Rolandi, G., Gans, P.B., Calvert, A., Bohrson, W.A., Spera, F.J., Belkin, H.E., 2001. New constraints on the pyroclastic eruptive history of the Campanian volcanic Plain (Italy). Mineralogy and Petrology 73, 47-65.
19. Druitt, T.H., Edwards, L., Mellors, R.M., Pyle, D.M., Sparks, R.S.J., Lanphere, M., Davies, M., Barreirio, B., 1999. Santorini Volcano. Geological Society, London, Memoirs 19.
20. Filippou, A., 2014. Minerochemical study of rhyolitic lavas with perlitic texture from the Island of Milos. MSc thesis, University of Patras, Patras, Greece (in Greek).

21. Fletcher, W.J., Müller, U.C., Koutsodendris, A., Christanis, K., Pross, J., 2013. A centennial-scale record of vegetation and climate variability from 312 to 240 ka (Marine Isotope Stages 9c–a, 8 and 7e) from Tenaghi Philippon, NE Greece. Quaternary Science Reviews 78, 108-125.

22. Fuller, S.A., 2015. Distribution of tephra from the 1650 AD submarine eruption of Kolumbo volcano, Greece. MSc thesis, University of Rhode Island, Ann Arbor, USA.

23. Fytikas, M., Giuliani, O., Innocenti, F., Marinelli, G., Mazzuoli, R., 1976. Geochronological data on recent magmatism of the Aegean Sea. Tectonophysics 31, T29-T34.

24. Fytikas, M., Innocenti, F., Kolios, N., Manetti, P., Mazzuoli, R., Poli, G., Rita, F., Villari, L., 1986. Volcanology and petrology of volcanic products from the island of Milos and neighbouring islets. Journal of Volcanology and Geothermal Research 28, 297-317.

25. Gaitanakis, P., Dietrich, V., 1995. Geological map of Methana peninsula 1: 25 000. ETH, Zürich.

26. Giaccio, B., Castorina, F., Nomade, S., Scardia, G., Voltaggio, M., Sagnotti, L., 2013. Revised chronology of the Sulmona lacustrine succession, central Italy. Journal of Quaternary Science 28, 545-551.

27. Giaccio, B., Galli, P., Peronace, E., Arienzo, I., Nomade, S., Cavinato, G.P., Mancini, M., Messina, P., Sottili, G., 2014. A 560-440 ka tephra record from the Mercure Basin, southern Italy: volcanological and tephrostratigraphic implications. Journal of Quaternary Science 29, 232-248.

28. Giaccio, B., Hajdas, I., Isaia, R., Deino, A., Nomade, S., 2017a. High-precision ^{14}C and $^{40}Ar/^{39}Ar$ dating of the Campanian Ignimbrite (Y-5) reconciles the time-scales of climatic-cultural processes at 40 ka. Scientific Reports 7, 45940.

29. Giaccio, B., Niespolo, E.M., Pereira, A., Nomade, S., Renne, P.R., Albert, P.G., Arienzo, I., Regattieri, E., Wagner, B., Zanchetta, G., Gaeta, M., Galli, P., Mannella, G., Peronace, E., Sottili, G., Florindo, F., Leicher, N., Marra, F., Tomlinson, E.L., 2017b. First integrated tephrochronological record for the last similar to 190 kyr from the Fucino Quaternary lacustrine succession, central Italy. Quaternary Science Reviews 158, 211-234.

30. Hunt, J.B., Hill, P.G., 1996. An inter-laboratory comparison of the electron probe microanalysis of glass geochemistry. Quaternary International 34-36, 229-241.

31. Jensen, B.J.L., Pyne-O'Donnell, S., Plunkett, G., Froese, D.G., Hughes, P.D.M., Sigl, M., McConnell, J.R., Amesbury, M.J., Blackwell, P.G., van den Bogaard, C., Buck, C.E., Charman, D.J., Clague, J.J., Hall, V.A., Koch, J., Mackay, H., Mallon, G., McColl, L., Pilcher, J.R., 2014. Transatlantic distribution of the Alaskan White River Ash. Geology 42, 875-878.

32. Jochum, K.P., Stoll, B., Herwig, K., Willbold, M., Hofmann, A.W., Amini, M., Aarburg, S., Abouchami, W., Hellebrand, E., Mocek, B., Raczek, I., Stracke, A., Alard, O., Bouman, C., Becker, S., Dücking, M., Brätz, H., Klemd, R., de Bruin, D., Canil, D., Cornell, D., de Hoog, C.-J., Dalpé, C., Danyushevsky, L., Eisenhauer, A., Gao, Y., Snow, J.E., Groschopf, N., Günther, D., Latkoczy, C., Guillong, M., Hauri, E.H., Höfer, H.E., Lahaye, Y., Horz, K., Jacob, D.E., Kasemann, S.A., Kent, A.J.R., Ludwig, T., Zack, T., Mason, P.R.D., Meixner, A., Rosner, M., Misawa, K., Nash, B.P., Pfänder, J., Premo, W.R., Sun, W.D., Tiepolo, M., Vannucci, R., Vennemann, T., Wayne, D., Woodhead, J.D., 2006. MPI-DING reference glasses for in situ microanalysis: New reference values for element concentrations and isotope ratios. Geochemistry, Geophysics, Geosystems 7, Q02008.

33. Jochum, K.P., Weis, U., Stoll, B., Kuzmin, D., Yang, Q., Raczek, I., Jacob, D.E., Stracke, A., Birbaum, K., Frick, D.A., Günther, D., Enzweiler, J., 2011.

Determination of reference values for NIST SRM 610–617 glasses following ISO guidelines. Geostandards and Geoanalytical Research 35, 397-429.

34. Kalaitzidis, S., 2007. Peat formation and evolution of peatlands in Greece. PhD thesis, University of Patras, Patras, Greece (in Greek).

35. Kalaitzidis, S., Christanis, K., 2002. Mineral matter in the Philippi peat in relation to peat/lignite-forming conditions in Greece. Energy Sources 24, 69-81.

36. Karátson, D., Wulf, S., Veres, D., Magyari, E.K., Gertisser, R., Timar-Gabor, A., Novothny, A., Telbisz, T., Szalai, Z., Anechitei-Deacu, V., Appelt, O., Bormann, M., Jánosi, C., Hubay, K., Schäbitz, F., 2016. The latest explosive eruptions of Ciomadul (Csomad) volcano, East Carpathians – A tephrostratigraphic approach for the 51–29 ka BP time interval. Journal of Volcanology and Geothermal Research 319, 29-51.

37. Keller, J., Ryan, W.B.F., Ninkovich, D., Altherr, R., 1978. Explosive volcanic activity in the Mediterranean over the past 200,000 yr as recorded in deep-sea sediments. Geological Society of America Bulletin 89, 591-604.

38. Koukouzas, N.K., 1997. Rare earth elements in volcanic glass: A case study from Trachilas perlite deposit, Greece. Chemie der Erde 57, 351-362.

39. Koukouzas, N.K., Dunham, A.C., 1998. Glass composition of perlites from Milos, Kimolos and Kos islands (Greece). Bulletin of the Geological Society of Greece 32, 303-312.

40. Kousis, I., Koutsodendris, A., Peyron, O., Leicher, N., Francke, A., Wagner, B., Giaccio, B., Knipping, M., Pross, J., 2018. Centennial-scale vegetation dynamics and climate variability in SE Europe during Marine Isotope Stage 11 based on a pollen record from Lake Ohrid. Quaternary Science Reviews 190, 20-38.

41. Kuehn, S.C., Froese, D.G., Shane, P.A.R., 2011. The INTAV intercomparison of electron-beam microanalysis of glass by tephrochronology laboratories: Results and recommendations. Quaternary International 246, 19-47.
42. Lane, C.S., Chorn, B.T., Johnson, T.C., 2013. Ash from the Toba supereruption in Lake Malawi shows no volcanic winter in East Africa at 75 ka. Proceedings of the National Academy of Sciences 110, 8025-8029.
43. Langdon, P.G., Barber, K.E., 2004. Snapshots in time: precise correlations of peat-based proxy climate records in Scotland using mid-Holocene tephras. The Holocene 14, 21-33.
44. Le Bas, M.J., Le Maitre, R.W., Streckeisen, A., Zanettin, B., 1986. A chemical classification of volcanic rocks based on the total alkali-silica diagram. Journal of Petrology 27, 745-750.
45. Leicher, N., Zanchetta, G., Sulpizio, R., Giaccio, B., Wagner, B., Nomade, S., Francke, A., Del Carlo, P., 2016. First tephrostratigraphic results of the DEEP site record from Lake Ohrid (Macedonia and Albania). Biogeosciences 13, 2151-2178.
46. Lowe, D.J., 2011. Tephrochronology and its application: A review. Quaternary Geochronology 6, 107-153.
47. Lowe, J., Barton, N., Blockley, S., Ramsey, C.B., Cullen, V.L., Davies, W., Gamble, C., Grant, K., Hardiman, M., Housley, R., Lane, C.S., Lee, S., Lewis, M., MacLeod, A., Menzies, M., Müller, W., Pollard, M., Price, C., Roberts, A.P., Rohling, E.J., Satow, C., Smith, V.C., Stringer, C.B., Tomlinson, E.L., White, D., Albert, P., Arienzo, I., Barker, G., Borić, D., Carandente, A., Civetta, L., Ferrier, C., Guadelli, J.-L., Karkanas, P., Koumouzelis, M., Müller, U.C., Orsi, G., Pross, J., Rosi, M., Shalamanov-Korobar, L., Sirakov, N., Tzedakis, P.C., 2012. Volcanic ash layers illuminate the resilience of Neanderthals and early modern humans to natural

hazards. Proceedings of the National Academy of Sciences of the United States of America 109, 13532-13537.

48. Macdonald, R., Sumita, M., Schmincke, H.U., Bagiński, B., White, J.C., Ilnicki, S.S., 2015. Peralkaline felsic magmatism at the Nemrut volcano, Turkey: impact of volcanism on the evolution of Lake Van (Anatolia) IV. Contributions to Mineralogy and Petrology 169, 34.

49. Margari, V., Pyle, D.M., Bryant, C., Gibbard, P.L., 2007. Mediterranean tephra stratigraphy revisited: Results from a long terrestrial sequence on Lesvos Island, Greece. Journal of Volcanology and Geothermal Research 163, 34-54.

50. Marra, F., Sottili, G., Gaeta, M., Giaccio, B., Jicha, B., Masotta, M., Palladino, D.M., Deocampo, D.M., 2014. Major explosive activity in the Monti Sabatini Volcanic District (central Italy) over the 800-390 ka interval: geochronological-geochemical overview and tephrostratigraphic implications. Quaternary Science Reviews 94, 74-101.

51. Martrat, B., Grimalt, J.O., Shackleton, N.J., de Abreu, L., Hutterli, M.A., Stocker, T.F., 2007. Four climate cycles of recurring deep and surface water destabilizations on the Iberian margin. Science 317, 502-507.

52. Matsuda, J.-i., Senoh, K., Maruoka, T., Sato, H., Mitropoulos, P., 1999. K-Ar ages of the Aegean volcanic rocks and their implication for the arc-trench system. Geochemical Journal 33, 369-377.

53. Milner, A.M., Roucoux, K.H., Collier, R.E.L., Müller, U.C., Pross, J., Tzedakis, P.C., 2016. Vegetation responses to abrupt climatic changes during the Last Interglacial Complex (Marine Isotope Stage 5) at Tenaghi Philippon, NE Greece. Quaternary Science Reviews 154, 169-181.

54. Molnár, K., Harangi, S., Lukács, R., Dunkl, I., Schmitt, A.K., Kiss, B., Garamhegyi, T., Seghedi, I., 2018. The onset of the volcanism in the Ciomadul Volcanic Dome

Complex (Eastern Carpathians): Eruption chronology and magma type variation. Journal of Volcanology and Geothermal Research 354, 39-56.

55. Mommersteeg, H.J.P.M., Loutre, M.F., Young, R., Wijmstra, T.A., Hooghiemstra, H., 1995. Orbital forced frequencies in the 975 000 year pollen record from Tenagi Philippon (Greece). Climate Dynamics 11, 4-24.

56. Müller, U.C., Pross, J., Tzedakis, P.C., Gamble, C., Kotthoff, U., Schmiedl, G., Wulf, S., Christanis, K., 2011. The role of climate in the spread of modern humans into Europe. Quaternary Science Reviews 30, 273-279.

57. Nomade, S., Scaillet, S., Pastre, J.-F., Nehlig, P., 2012. Pyroclastic chronology of the Sancy stratovolcano (Mont-Dore, French Massif Central): New high-precision $^{40}Ar/^{39}Ar$ constraints. Journal of Volcanology and Geothermal Research 225-226, 1-12.

58. Palladino, D.M., Gaeta, M., Giaccio, B., Sottili, G., 2014. On the anatomy of magma chamber and caldera collapse: The example of trachy-phonolitic explosive eruptions of the Roman Province (central Italy). Journal of Volcanology and Geothermal Research 281, 12-26.

59. Pappalardo, L., Civetta, L., D'Antonio, M., Deino, A., Di Vito, M., Orsi, G., Carandente, A., de Vita, S., Isaia, R., Piochi, M., 1999. Chemical and Sr-isotopical evolution of the Phlegraean magmatic system before the Campanian Ignimbrite and the Neapolitan Yellow Tuff eruptions. Journal of Volcanology and Geothermal Research 91, 141-166.

60. Parrenin, F., Barnola, J.M., Beer, J., Blunier, T., Castellano, E., Chappellaz, J., Dreyfus, G., Fischer, H., Fujita, S., Jouzel, J., Kawamura, K., Lemieux-Dudon, B., Loulergue, L., Masson-Delmotte, V., Narcisi, B., Petit, J.R., Raisbeck, G., Raynaud, D., Ruth, U., Schwander, J., Severi, M., Spahni, R., Steffensen, J.P.,

Svensson, A., Udisti, R., Waelbroeck, C., Wolff, E., 2007. The EDC3 chronology for the EPICA Dome C ice core. Climate of the Past 3, 485-497.

61. Pasteels, P., Kolios, N., Boven, A., Saliba, E., 1986. Applicability of the K/Ar method to whole-rock samples of acid lava and pumice: Case of the Upper Pleistocene domes and pyroclasts on Kos Island, Aegean Sea, Greece. Chemical Geology 57, 145-154.
62. Pe, G.G., 1974. Volcanic rocks of Methana, South Aegean arc, Greece. Bulletin Volcanologique 38, 270-290.
63. Pe-Piper, G., Piper, D.J., 2002. The igneous rocks of Greece. The anatomy of an orogen. Gebrüder Borntraeger, Berlin, Stuttgart.
64. Pe-Piper, G., Moulton, B., 2008. Magma evolution in the Pliocene–Pleistocene succession of Kos, South Aegean arc (Greece). Lithos 106, 110-124.
65. Peccerillo, A., 2017. Cenozoic volcanism in the Tyrrhenian Sea region. Springer International Publishing, Cham, Switzerland.
66. Peccerillo, A., Taylor, S.R., 1976. Geochemistry of Eocene calc-alkaline volcanic rocks from the Kastamonu area, northern Turkey. Contributions to Mineralogy and Petrology 58, 63-81.
67. Petrosino, P., Jicha, B.R., Mazzeo, F.C., Russo Ermolli, E., 2014. A high resolution tephrochronological record of MIS 14-12 in the Southern Apennines (Acerno Basin, Italy). Journal of Volcanology and Geothermal Research 274, 34-50.
68. Petrosino, P., Jicha, B.R., Mazzeo, F.C., Ciaranfi, N., Girone, A., Maiorano, P., Marino, M., 2015. The Montalbano Jonico marine succession: An archive for distal tephra layers at the Early-Middle Pleistocene boundary in southern Italy. Quaternary International 383, 89-103.
69. Platevoet, B., Elitok, Ö., Guillou, H., Bardintzeff, J.-M., Yagmurlu, F., Nomade, S., Poisson, A., Deniel, C., Özgür, N., 2014. Petrology of Quaternary volcanic rocks

and related plutonic xenoliths from Gölcük volcano, Isparta Angle, Turkey: Origin and evolution of the high-K alkaline series. Journal of Asian Earth Sciences 92, 53-76.

70. Poli, S., Chiesa, S., Gillot, P.-Y., Gregnanin, A., Guichard, F., 1987. Chemistry versus time in the volcanic complex of Ischia (Gulf of Naples, Italy): evidence of successive magmatic cycles. Contributions to Mineralogy and Petrology 95, 322-335.

71. Ponomareva, V., Portnyagin, M., Davies, S.M., 2015. Tephra without borders: Far-reaching clues into past explosive eruptions. Frontiers in Earth Science 3, 83.

72. Pross, J., Tzedakis, P., Schmiedl, G., Christanis, K., Hooghiemstra, H., Müller, U.C., Kotthoff, U., Kalaitzidis, S., Milner, A., 2007. Tenaghi Philippon (Greece) revisited: Drilling a continuous lower-latitude terrestrial climate archive of the last 250,000 years. Scientific Drilling 5, 44-46.

73. Pross, J., Kotthoff, U., Müller, U., Peyron, O., Dormoy, I., Schmiedl, G., Kalaitzidis, S., Smith, A., 2009. Massive perturbation in terrestrial ecosystems of the Eastern Mediterranean region associated with the 8.2 kyr B.P. climatic event. Geology 37, 887-890.

74. Pross, J., Koutsodendris, A., Christanis, K., Fischer, T., Fletcher, W.J., Hardiman, M., Kalaitzidis, S., Knipping, M., Kotthoff, U., Milner, A.M., Müller, U.C., Schmiedl, G., Siavalas, G., Tzedakis, P.C., Wulf, S., 2015. The 1.35-Ma-long terrestrial climate archive of Tenaghi Philippon, northeastern Greece: Evolution, exploration, and perspectives for future research. Newsletters on Stratigraphy 48, 253-276.

75. Pyne-O'Donnell, S., 2011. The taphonomy of Last Glacial–Interglacial Transition (LGIT) distal volcanic ash in small Scottish lakes. Boreas 40, 131-145.

76. Railsback, L.B., Gibbard, P.L., Head, M.J., Voarintsoa, N.R.G., Toucanne, S., 2015. An optimized scheme of lettered marine isotope substages for the last 1.0

million years, and the climatostratigraphic nature of isotope stages and substages. Quaternary Science Reviews 111, 94-106.

77. Regattieri, E., Giaccio, B., Galli, P., Nomade, S., Peronace, E., Messina, P., Sposato, A., Boschi, C., Gemelli, M., 2016. A multi-proxy record of MIS 11-12 deglaciation and glacial MIS 12 instability from the Sulmona basin (central Italy). Quaternary Science Reviews 132, 129-145.

78. Rolandi, G., Bellucci, F., Heizler, M.T., Belkin, H.E., De Vivo, B., 2003. Tectonic controls on the genesis of ignimbrites from the Campanian Volcanic Zone, southern Italy. Mineralogy and Petrology 79, 3-31.

79. Roucoux, K.H., Tzedakis, P.C., de Abreu, L., Shackleton, N.J., 2006. Climate and vegetation changes 180,000 to 345,000 years ago recorded in a deep-sea core off Portugal. Earth and Planetary Science Letters 249, 307-325.

80. Sandri, L., Costa, A., Selva, J., Tonini, R., Macedonio, G., Folch, A., Sulpizio, R., 2016. Beyond eruptive scenarios: assessing tephra fallout hazard from Neapolitan volcanoes. Scientific Reports 6, 24271.

81. Satow, C., Tomlinson, E.L., Grant, K.M., Albert, P.G., Smith, V.C., Manning, C.J., Ottolini, L., Wulf, S., Rohling, E.J., Lowe, J.J., Blockley, S.P.E., Menzies, M.A., 2015. A new contribution to the Late Quaternary tephrostratigraphy of the Mediterranean: Aegean Sea core LC21. Quaternary Science Reviews 117, 96-112.

82. Schmincke, H.-U., Sumita, M., 2014. Impact of volcanism on the evolution of Lake Van (eastern Anatolia) III: Periodic (Nemrut) vs. episodic (Süphan) explosive eruptions and climate forcing reflected in a tephra gap between ca. 14 ka and ca. 30 ka. Journal of Volcanology and Geothermal Research 285, 195-213.

83. Şen, E., Kürkcüoğlu, B., Aydar, E., Gourgaud, A., Vincent, P.M., 2003. Volcanological evolution of Mount Erciyes stratovolcano and origin of the Valibaba

Tepe ignimbrite (Central Anatolia, Turkey). Journal of Volcanology and Geothermal Research 125, 225-246.

84. Smith, V.C., Isaia, R., Pearce, N.J.G., 2011. Tephrostratigraphy and glass compositions of post-15 kyr Campi Flegrei eruptions: implications for eruption history and chronostratigraphic markers. Quaternary Science Reviews 30, 3638-3660.

85. Smith, V.C., Isaia, R., Engwell, S.L., Albert, P.G., 2016. Tephra dispersal during the Campanian Ignimbrite (Italy) eruption: implications for ultra-distal ash transport during the large caldera-forming eruption. Bulletin of Volcanology 78, 45.

86. St. Seymour, K., Christanis, K., Bouzinos, A., Papazisimou, S., Papatheodorou, G., Moran, E., Denes, G., 2004. Tephrostratigraphy and tephrochronology in the Philippi peat basin, Macedonia, Northern Hellas (Greece). Quaternary International 121, 53-65.

87. Sulpizio, R., Zanchetta, G., Caron, B., Dellino, P., Mele, D., Giaccio, B., Insinga, D., Paterne, M., Siani, G., Costa, A., Macedonio, G., Santacroce, R., 2014. Volcanic ash hazard in the Central Mediterranean assessed from geological data. Bulletin of Volcanology 76.

88. Sumita, M., Schmincke, H.-U., 2013a. Impact of volcanism on the evolution of Lake Van I: evolution of explosive volcanism of Nemrut Volcano (eastern Anatolia) during the past >400,000 years. Bulletin of Volcanology 75, 714.

89. Sumita, M., Schmincke, H.-U., 2013b. Impact of volcanism on the evolution of Lake Van II: Temporal evolution of explosive volcanism of Nemrut Volcano (eastern Anatolia) during the past ca. 0.4 Ma. Journal of Volcanology and Geothermal Research 253, 15-34.

90. Tamburrino, S., Insinga, D.D., Sprovieri, M., Petrosino, P., Tiepolo, M., 2012. Major and trace element characterization of tephra layers offshore Pantelleria

Island: insights into the last 200 ka of volcanic activity and contribution to the Mediterranean tephrochronology. Journal of Quaternary Science 27, 129-140.

91. Tomlinson, E.L., Arienzo, I., Civetta, L., Wulf, S., Smith, V.C., Hardiman, M., Lane, C.S., Carandente, A., Orsi, G., Rosi, M., Muller, W., Menzies, M.A., 2012a. Geochemistry of the Phlegraean Fields (Italy) proximal sources for major Mediterranean tephras: Implications for the dispersal of Plinian and co-ignimbritic components of explosive eruptions. Geochimica et Cosmochimica Acta 93, 102-128.

92. Tomlinson, E.L., Kinvig, H.S., Smith, V.C., Blundy, J.D., Gottsmann, J., Müller, W., Menzies, M.A., 2012b. The Upper and Lower Nisyros Pumices: Revisions to the Mediterranean tephrostratigraphic record based on micron-beam glass geochemistry. Journal of Volcanology and Geothermal Research 243, 69-80.

93. Tomlinson, E.L., Albert, P.G., Wulf, S., Brown, R.J., Smith, V.C., Keller, J., Orsi, G., Bourne, A.J., Menzies, M.A., 2014. Age and geochemistry of tephra layers from Ischia, Italy: constraints from proximal-distal correlations with Lago Grande di Monticchio. Journal of Volcanology and Geothermal Research 287, 22-39.

94. Tomlinson, E.L., Smith, V.C., Albert, P.G., Aydar, E., Civetta, L., Cioni, R., Cubukcu, E., Gertisser, R., Isaia, R., Menzies, M.A., Orsi, G., Rosi, M., Zanchetta, G., 2015. The major and trace element glass compositions of the productive Mediterranean volcanic sources: tools for correlating distal tephra layers in and around Europe. Quaternary Science Reviews 118, 48-66.

95. Tzedakis, P.C., Hooghiemstra, H., Pälike, H., 2006. The last 1.35 million years at Tenaghi Philippon: revised chronostratigraphy and long-term vegetation trends. Quaternary Science Reviews 25, 3416-3430.

96. Vakhrameeva, P., Koutsodendris, A., Wulf, S., Fletcher, W.J., Appelt, O., Knipping, M., Gertisser, R., Trieloff, M., Pross, J., 2018. The cryptotephra record of the

Marine Isotope Stage 12 to 10 interval (460–335 ka) at Tenaghi Philippon, Greece: Exploring chronological markers for the Middle Pleistocene of the Mediterranean region. Quaternary Science Reviews 200, 313-333.

97. Van der Wiel, A.M., Wijmstra, T.A., 1987a. Palynology of the lower part (78–120 m) of the core Tenaghi Philippon II, Middle Pleistocene of Macedonia, Greece. Review of Palaeobotany and Palynology 52, 73-88.

98. Van der Wiel, A.M., Wijmstra, T.A., 1987b. Palynology of the 112.8–197.8 m interval of the core Tenaghi Philippon III, Middle Pleistocene of Macedonia. Review of Palaeobotany and Palynology 52, 89-117.

99. Watson, E.J., Swindles, G.T., Lawson, I.T., Savov, I.P., 2015. Spatial variability of tephra and carbon accumulation in a Holocene peatland. Quaternary Science Reviews 124, 248-264.

100. Weltje, G.J., Bloemsma, M.R., Tjallingii, R., Heslop, D., Röhl, U., Croudace, I.W., 2015. Prediction of geochemical composition from XRF core scanner data: A new multivariate approach including automatic selection of calibration samples and quantification of uncertainties, in: Croudace, I.W., Rothwell, R.G. (Eds.), Micro-XRF studies of sediment cores. Developments in paleoenvironmental research, Vol. 17. Springer, Dordrecht, pp. 507-534.

101. Wijmstra, T.A., 1969. Palynology of the first 30 metres of a 120 m deep section in northern Greece. Acta Botanica Neerlandica 18, 511-527.

102. Wijmstra, T.A., Smit, A., 1976. Palynology of the middle part (30–78 metres) of the 120 m deep section in northern Greece (Macedonia). Acta Botanica Neerlandica 25, 297-312.

103. Wijmstra, T.A., Groenhart, M.C., 1983. Record of 700,000 years vegetational history in Eastern Macedonia (Greece). Revista de la Academia Colombiana Ciencias Exactas, Fisicas y Naturales 15, 87-98.

104. Wolff-Boenisch, D., Gislason, S.R., Oelkers, E.H., Putnis, C.V., 2004. The dissolution rates of natural glasses as a function of their composition at pH 4 and 10.6, and temperatures from 25 to 74°C. Geochimica et Cosmochimica Acta 68, 4843-4858.

105. Wulf, S., Kraml, M., Brauer, A., Keller, J., Negendank, J.F.W., 2004. Tephrochronology of the 100 ka lacustrine sediment record of Lago Grande di Monticchio (southern Italy). Quaternary International 122, 7-30.

106. Wulf, S., Keller, J., Paterne, M., Mingram, J., Lauterbach, S., Opitz, S., Sottili, G., Giaccio, B., Albert, P.G., Satow, C., Tomlinson, E.L., Viccaro, M., Brauer, A., 2012. The 100–133 ka record of Italian explosive volcanism and revised tephrochronology of Lago Grande di Monticchio. Quaternary Science Reviews 58, 104-123.

107. Wulf, S., Hardiman, M., Staff, R.A., Koutsodendris, A., Appelt, O., Blockley, S.P.E., Lowe, J.J., Manning, C.J., Ottolini, L., Schmitt, A.K., Smith, V.C., Tomlinson, E.L., Vakhrameeva, P., Knipping, M., Kotthoff, U., Milner, A.M., Müller, U.C., Christanis, K., Kalaitzidis, S., Tzedakis, C., Schmiedl, G., Pross, J., 2018. The marine isotope stage 1–5 cryptotephra record of Tenaghi Philippon, Greece: Towards a detailed tephrostratigraphic framework for the Eastern Mediterranean region. Quaternary Science Reviews 186, 236-262.

108. Zanchetta, G., Sulpizio, R., Roberts, N., Cioni, R., Eastwood, W.J., Siani, G., Caron, B., Paterne, M., Santacroce, R., 2011. Tephrostratigraphy, chronology and climatic events of the Mediterranean basin during the Holocene: An overview. The Holocene 21, 33-52.

109. Zouzias, D., St. Seymour, K., 2008. Consanguineous geochemistry of the Kos Plateau and Tilos D and E Pumices, Aegean Volcanic Arc, Hellas. Neues Jahrbuch für Mineralogie – Abhandlungen 184, 231-241.

110. Zouzias, D., St. Seymour, K., 2013. Kos Plateau Tuff (KPT) on Kalymnos island, Aegean volcanic arc: A geochemical approach. Journal of Volcanology and Seismology 7, 293-312.

Figure captions

Figure 1: Map of the Central and Eastern Mediterranean regions showing the locations of Tenaghi Philippon and the main volcanic centers active or potentially active during MIS 9–7e: A, Aeolian Islands; Ac, Acigöl; C, Ciomadul; CA, Colli Albani; CF, Campi Flegrei; Ch, Christiana Islands; E, Etna; ED, Erciyes Dagi; G, Gölcük; HD, Hasan Dagi; Is, Ischia; K, Kos; M, Milos and Antimilos; Me, Methana; N, Nemrut; P, Pantelleria; R, Roccamonfina; S, Sabatini; Sn, Sancy; St, Santorini; Sü, Süphan; V, Vico; Vs, Vulsini.

Figure 2: Lithostratigraphy, glass-shard counts, tree-pollen percentages, and normalized Si_{CLR} intensities for the overlap intervals of Tenaghi Philippon cores TP-2005 and TP-2009. Cryptotephra layers occurring in both cores are highlighted in color (see Fig. 3 for details on color coding).

Figure 3: Cryptotephra record with glass-shard counts plotted against tree-pollen data for the MIS 9–7e interval at Tenaghi Philippon. Cryptotephra layers are color-coded to indicate their provenance as inferred in this study. MIS boundaries after Fletcher et al. (2013).

Figure 4: Cryptotephra layers within the MIS 9–7e interval at Tenaghi Philippon plotted in (**A**) total alkali *vs.* silica diagram (Le Bas et al., 1986); (**B**) K_2O *vs.* SiO_2 diagram (Peccerillo and Taylor, 1976); (**C**) K_2O/Na_2O *vs.* SiO_2 diagram; a close-up shows classification of Italian volcanic rocks based on K_2O/Na_2O ratio (modified after Peccerillo,

2017); (**D**) Rb *vs.* Y+Nb and Nb/Rb *vs.* Th/Rb diagrams (Tomlinson et al., 2015) discriminating anorogenic, active-subduction and post-subduction tectonic settings. Tephras are grouped into color-coded geochemical populations. Rock types: A – andesite; B – basalt; BA – basaltic andesite; BTA – basaltic trachyandesite; D – dacite; F – foidite; L – latite; P – phonolite; PB – picrobasalt; PT – phonotephrite; R – rhyolite; S – shoshonite; SB – shoshonitic basalt; TB – tephrite or basanite; TP – tephriphonolite; Tr – trachyte; TrA – trachyandesite; TrB – trachybasalt; TrD – trachydacite.

Figure 5: (**A**) K_2O/Na_2O *vs.* SiO_2 and (**B**) Cl *vs*. CaO/FeO (modified after Giaccio et al., 2017b) diagrams showing comparison of trachyphonolitic cryptotephra layers (POP1) from Tenaghi Philippon with potential Italian volcanic sources; (**C**) major- and trace-element plots supporting correlation of the trachyphonolitic cryptotephra layers with Campanian volcanoes and individual eruptions. Asterisk (*) marks tephras with Campanian geochemical characteristics that are older than proximal Campanian volcanic rocks (c. 290 ka); cryptotephra layer TP09-70.45 from the MIS 12–10 interval at Tenaghi Philippon (Vakhrameeva et al., 2018) is shown separately. Data sources: Campi Flegrei (Campanian Ignimbrite, pre- and post-Campanian Ignimbrite series) – Smith et al. (2011, 2016), Tomlinson et al. (2012a); Etna – Wulf et al. (2004, 2012); Albert et al. (2013); Ischia – Tomlinson et al. (2014, 2015); Old Campanian Tephras – Giaccio et al. (2013, 2014), Petrosino et al. (2014, 2015), Leicher et al. (2016); Pantelleria – Tamburrino et al. (2012), Tomlinson et al. (2015); Roccamonfina – Giaccio et al. (2014), Regattieri et al. (2016); Sabatini – Giaccio et al. (2014), Marra et al. (2014), Palladino et al. (2014); Taurano Ignimbrite – Amato et al. (2018); Vico – Marra et al. (2014), Palladino et al. (2014), Regattieri et al. (2016); Vulsini – Palladino et al. (2014).

Figure 6: Major-element bivariate plots showing (**A**) comparison of dacitic (POP2) and rhyolitic (POP3) cryptotephra layers from Tenaghi Philippon with Santorini pyroclastic units; (**B**) comparison of rhyolitic (POP4, POP5 and POP6) cryptotephra layers from Tenaghi Philippon with potential Middle Pleistocene volcanic and eruptive sources from the Aegean Arc. Data sources: Kos – Dalabakis and Vougioukalakis (1993), Pe-Piper and Moulton (2008), Zouzias and St. Seymour (2008, 2013); Methana – Pe (1974); Milos – Koukouzas (1997), Koukouzas and Dunham (1998), Filippou (2014); Santorini – Vakhrameeva et al. (2018).

Figure 7: (**A**) Major- and (**B**) trace-element bivariate plots showing comparison of dacitic and rhyolitic cryptotephra layers from Tenaghi Philippon with volcanic centers in the Mediterranean region: Aegean Arc, including Quaternary rocks of Methana, Milos, Kolumbo, Kos, Nisyros, Yali, and (plotted separately) Santorini; Aeolian Islands, including Salina and Lipari; western (Gölcük), central (Acigöl; Erciyes Dagi), eastern (Nemrut, Süphan) Anatolia and Carpathians (Ciomadul). Data sources: Aegean Arc – Pe (1974), Dalabakis and Vougioukalakis (1993), Koukouzas (1997), Koukouzas and Dunham (1998), Margari et al. (2007), Aksu et al. (2008), Pe-Piper and Moulton (2008), Zouzias and St. Seymour (2008, 2013), Tomlinson et al. (2012b), Cantner et al. (2014), Filippou (2014), Fuller (2015); Santorini – Druitt et al. (1999), Margari et al. (2007), Satow et al. (2015), Tomlinson et al. (2015), Vakhrameeva et al. (2018); Salina and Lipari – Albert et al. (2012, 2017); western and central Anatolia – Tomlinson et al. (2015); eastern Anatolia – Sumita and Schmincke (2013a, b), Schmincke and Sumita (2014), Macdonald et al. (2015); Carpathians – Karátson et al. (2016).

Table titles

Table 1: Summary of cryptotephra samples in the MIS 9–7e interval of cores TP-2005 and TP-2009 including glass-shard counts, compositional groups, proposed origin, and estimated ages. Samples marked with an asterisk were not geochemically analyzed.

Table 2: Representative EPMA (non-normalized) and SIMS glass data of cryptotephra samples in the MIS 9–7e interval of cores TP-2005 and TP-2009.

Supplementary files

Supplement 1: Full EPMA and SIMS glass analytical data of cryptotephra layers from Tenaghi Philippon.

Supplement 2: Complementary tables and bivariate elemental plots supporting the interpretation.

Figure 1

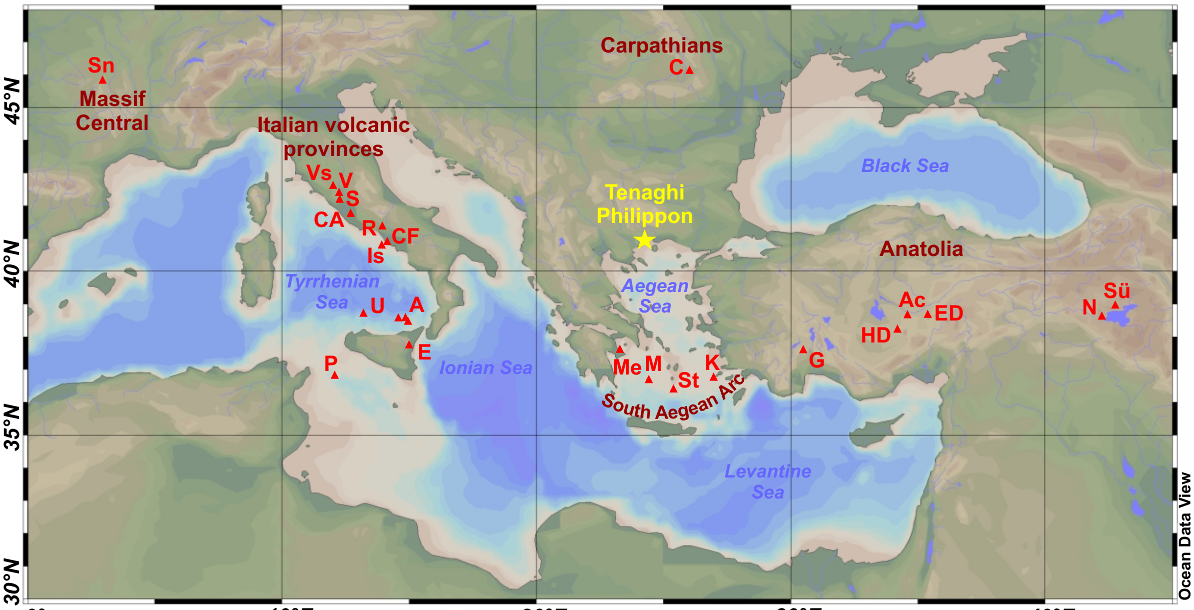

Carpathians
C
Sn
Massif Central
Italian volcanic provinces
Vs
V
S
CA
R
CF
Is
Tyrrhenian Sea
U
A
E
P
Ionian Sea
Tenaghi Philippon
Aegean Sea
Black Sea
Anatolia
Me
M
St
K
South Aegean Arc
G
HD
Ac
ED
N
Sü
Levantine Sea
45°N
40°N
35°N
30°N
0°
10°E
20°E
30°E
40°E
Ocean Data View

Figure 2

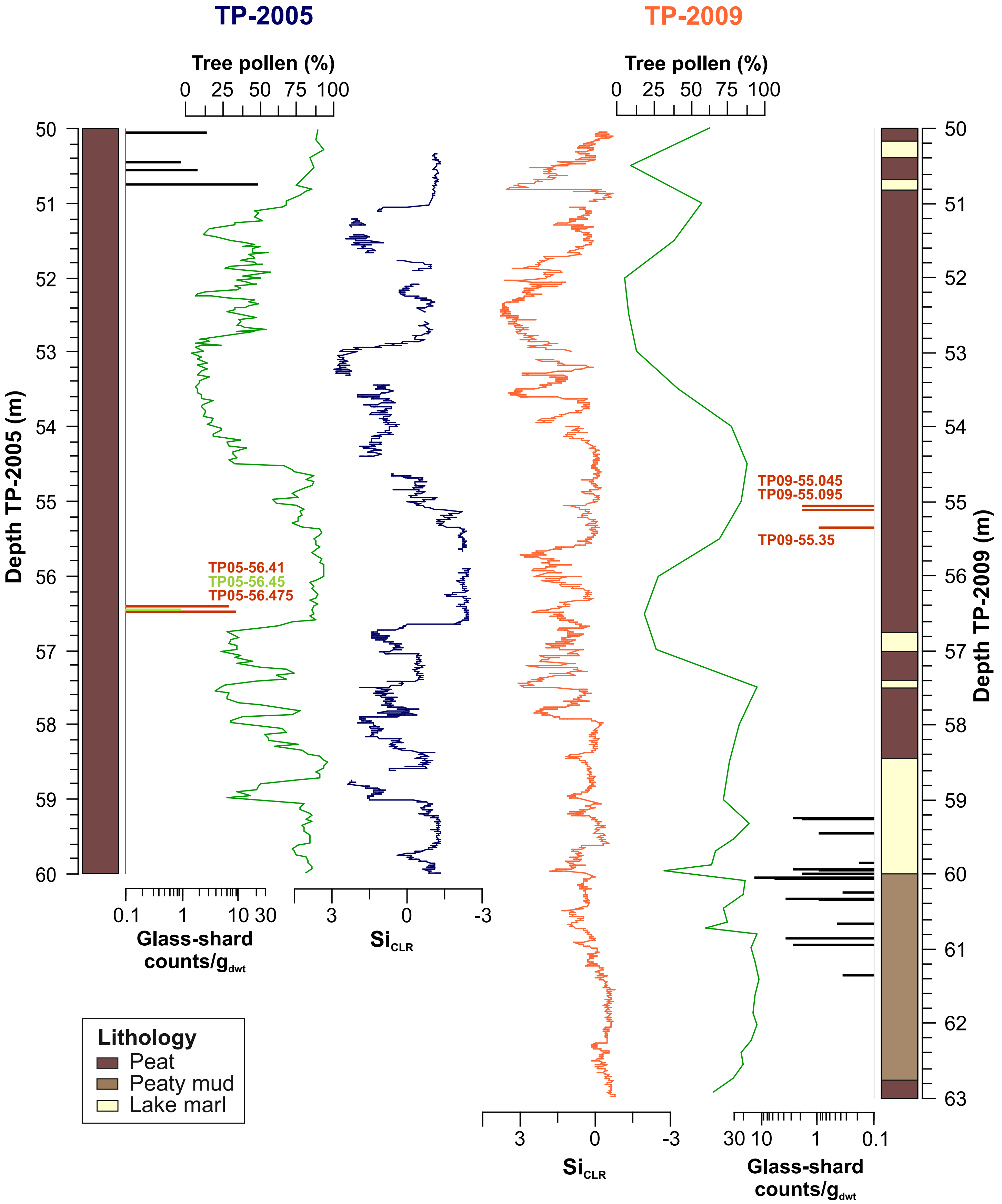

TP-2005
TP-2009
Tree pollen (%)
0 25 50 75 100
Tree pollen (%)
0 25 50 75 100
Depth TP-2005 (m)
Depth TP-2009 (m)
TP05-56.41
TP05-56.45
TP05-56.475
TP09-55.045
TP09-55.095
TP09-55.35
0.1 1 10 30
Glass-shard counts/g dwt
3 0 -3
Si CLR
3 0 -3
Si CLR
30 10 1 0.1
Glass-shard counts/g dwt
Lithology
Peat
Peaty mud
Lake marl

Figure 3

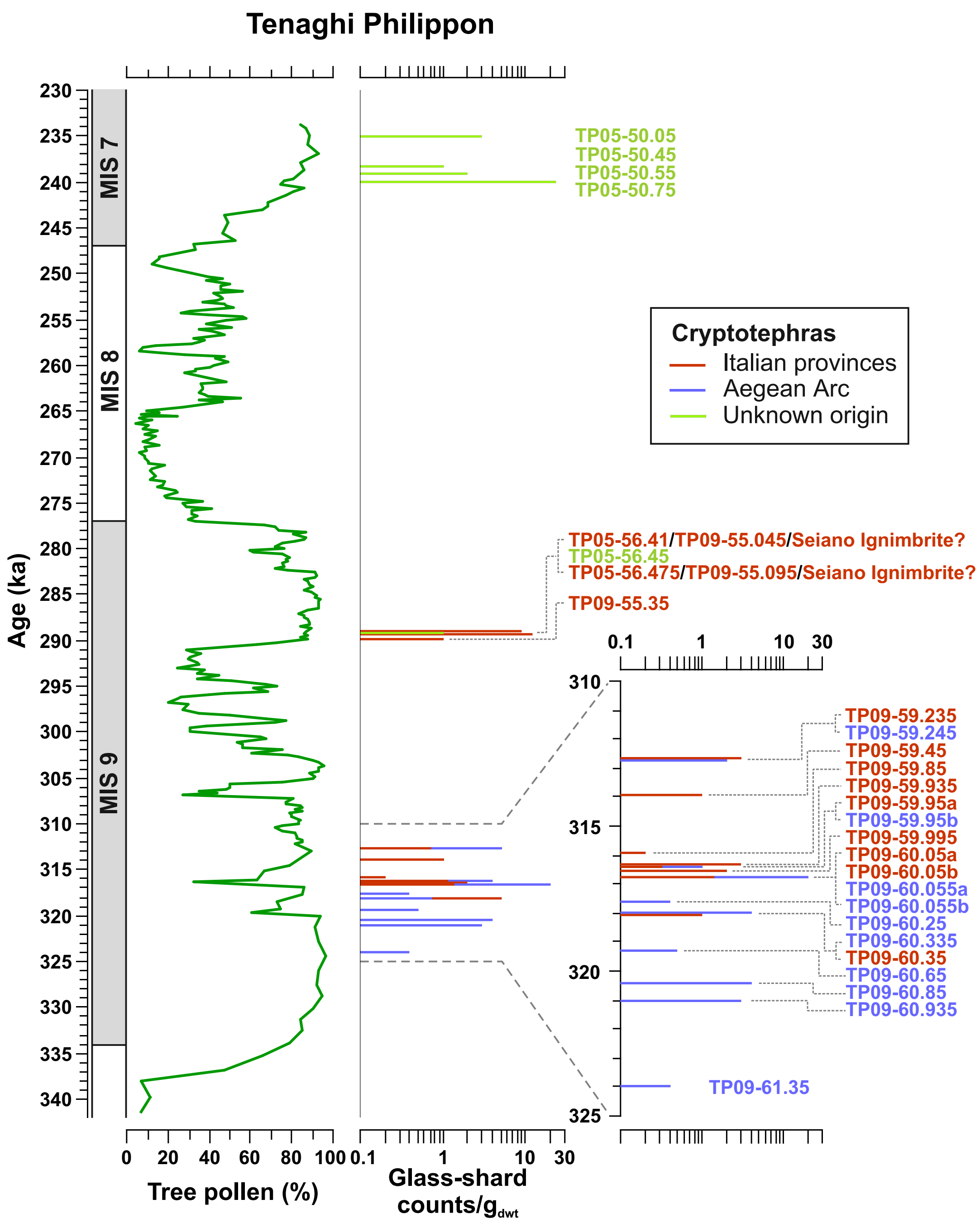

Tenaghi Philippon
Age (ka)
MIS 7
MIS 8
MIS 9
Tree pollen (%)
Glass-shard counts/g$_{dwt}$
Cryptotephras
Italian provinces
Aegean Arc
Unknown origin
TP05-50.05
TP05-50.45
TP05-50.55
TP05-50.75
TP05-56.41/TP09-55.045/Seiano Ignimbrite?
TP05-56.45
TP05-56.475/TP09-55.095/Seiano Ignimbrite?
TP09-55.35
TP09-59.235
TP09-59.245
TP09-59.45
TP09-59.85
TP09-59.935
TP09-59.95a
TP09-59.95b
TP09-59.995
TP09-60.05a
TP09-60.05b
TP09-60.055a
TP09-60.055b
TP09-60.25
TP09-60.335
TP09-60.35
TP09-60.65
TP09-60.85
TP09-60.935
TP09-61.35

Figure 4

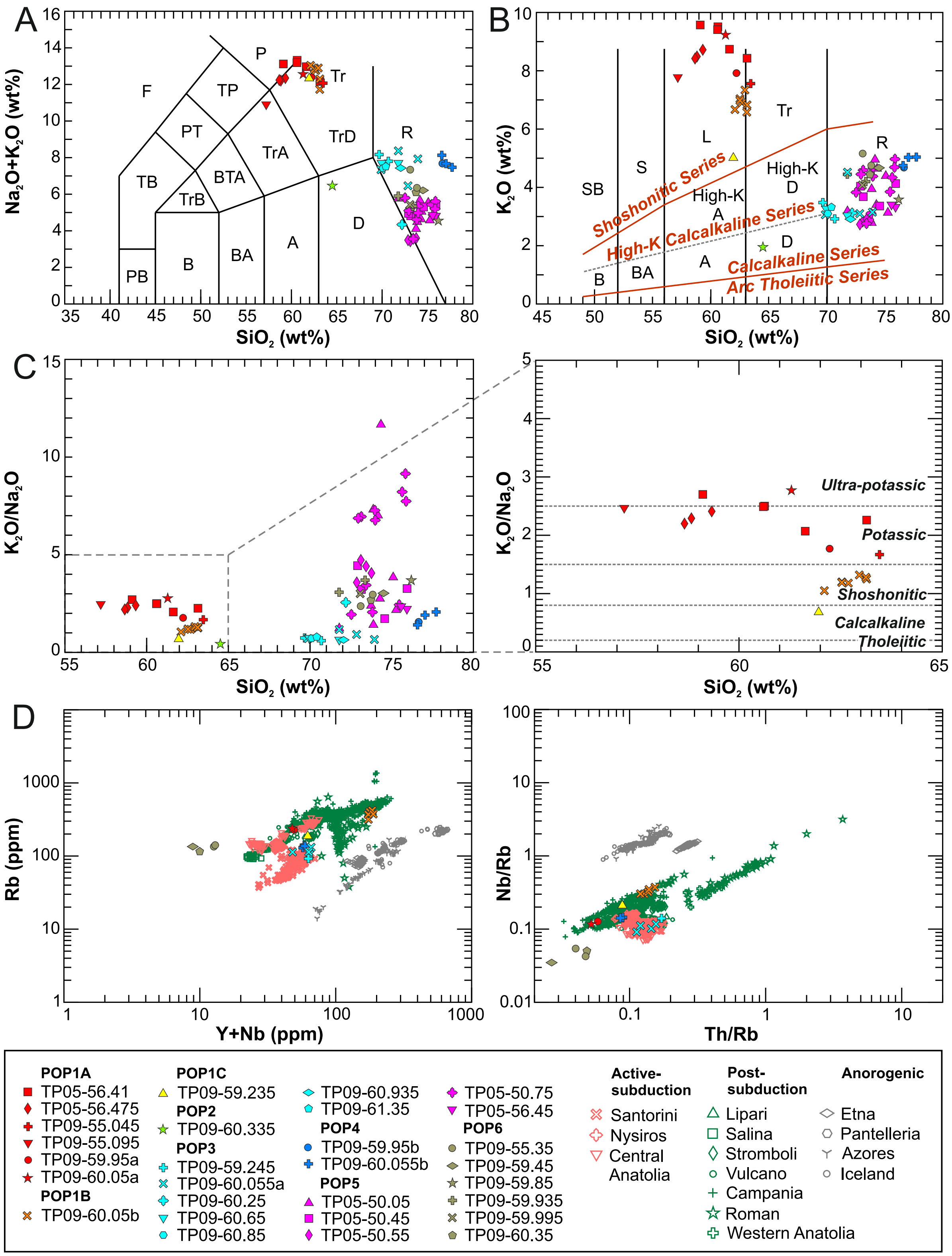

A
Na2O+K2O (wt%)
SiO2 (wt%)
F
P
TP
PT
TB
BTA
TrB
TrA
TrD
Tr
R
D
PB
B
BA
A
B
K2O (wt%)
SB
S
L
High-K A
High-K D
Shoshonitic Series
High-K Calcalkaline Series
Calcalkaline Series
Arc Tholeiitic Series
C
K2O/Na2O
Ultra-potassic
Potassic
Shoshonitic
Calcalkaline
Tholeiitic
D
Rb (ppm)
Y+Nb (ppm)
Nb/Rb
Th/Rb
POP1A
TP05-56.41
TP05-56.475
TP09-55.045
TP09-55.095
TP09-59.95a
TP09-60.05a
POP1B
TP09-60.05b
POP1C
TP09-59.235
POP2
TP09-60.335
POP3
TP09-59.245
TP09-60.055a
TP09-60.25
TP09-60.65
TP09-60.85
TP09-60.935
TP09-61.35
POP4
TP09-59.95b
TP09-60.055b
POP5
TP05-50.05
TP05-50.45
TP05-50.55
TP05-50.75
TP05-56.45
POP6
TP09-55.35
TP09-59.45
TP09-59.85
TP09-59.935
TP09-59.995
TP09-60.35
Active-subduction
Santorini
Nysiros
Central Anatolia
Post-subduction
Lipari
Salina
Stromboli
Vulcano
Campania
Roman
Western Anatolia
Anorogenic
Etna
Pantelleria
Azores
Iceland

Figure 5

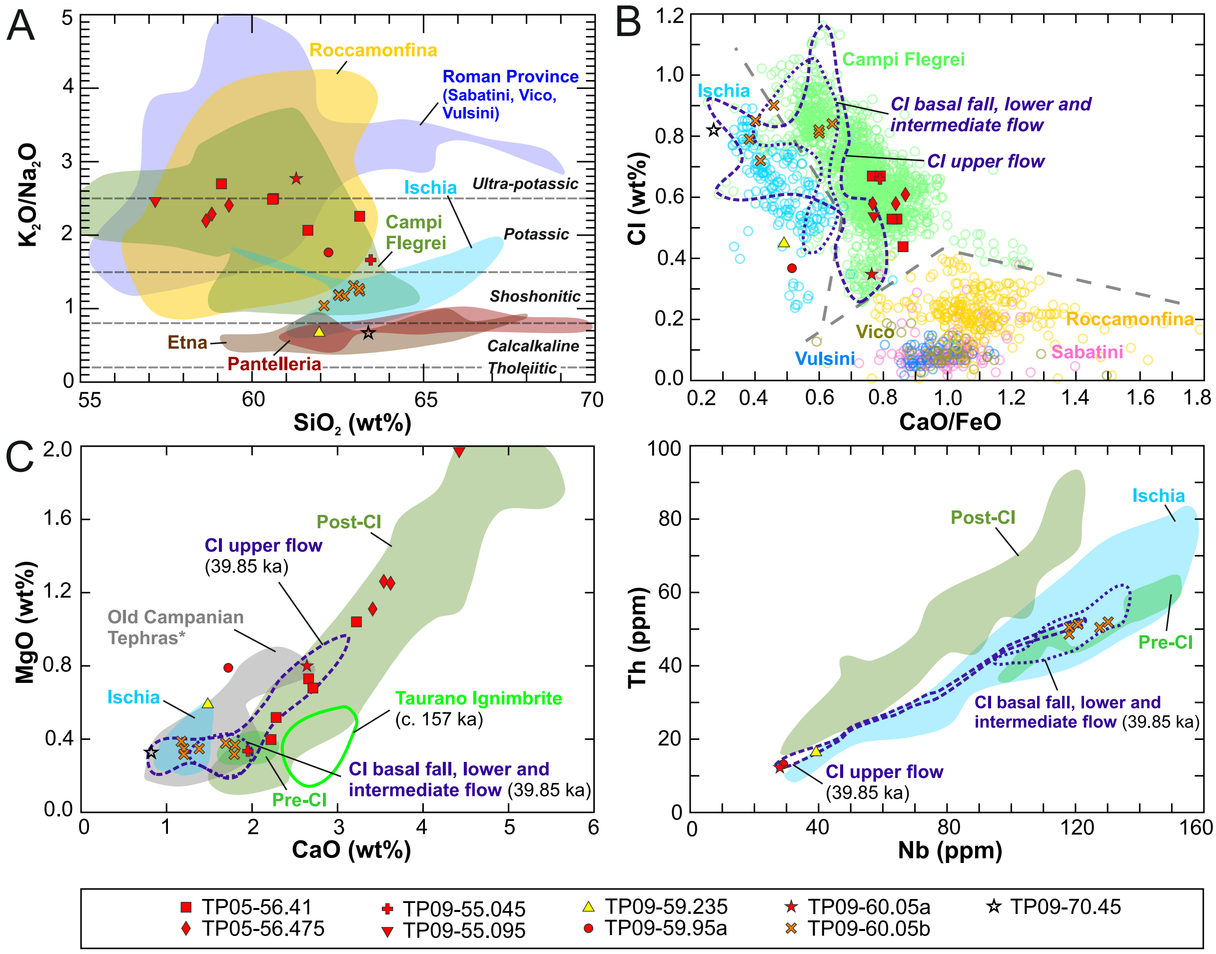

A
B
C
Roccamonfina
Roman Province (Sabatini, Vico, Vulsini)
Ischia
Ultra-potassic
Campi Flegrei
Potassic
Shoshonitic
Etna
Calcalkaline
Pantelleria
Tholeiitic
K_2O/Na_2O
SiO_2 (wt%)
Cl (wt%)
CaO/FeO
CI basal fall, lower and intermediate flow
CI upper flow
Vico
Vulsini
Sabatini
MgO (wt%)
CaO (wt%)
Post-CI
CI upper flow (39.85 ka)
Old Campanian Tephras*
Taurano Ignimbrite (c. 157 ka)
CI basal fall, lower and intermediate flow (39.85 ka)
Pre-CI
Th (ppm)
Nb (ppm)
TP05-56.41
TP05-56.475
TP09-55.045
TP09-55.095
TP09-59.235
TP09-59.95a
TP09-60.05a
TP09-60.05b
TP09-70.45

Figure 6

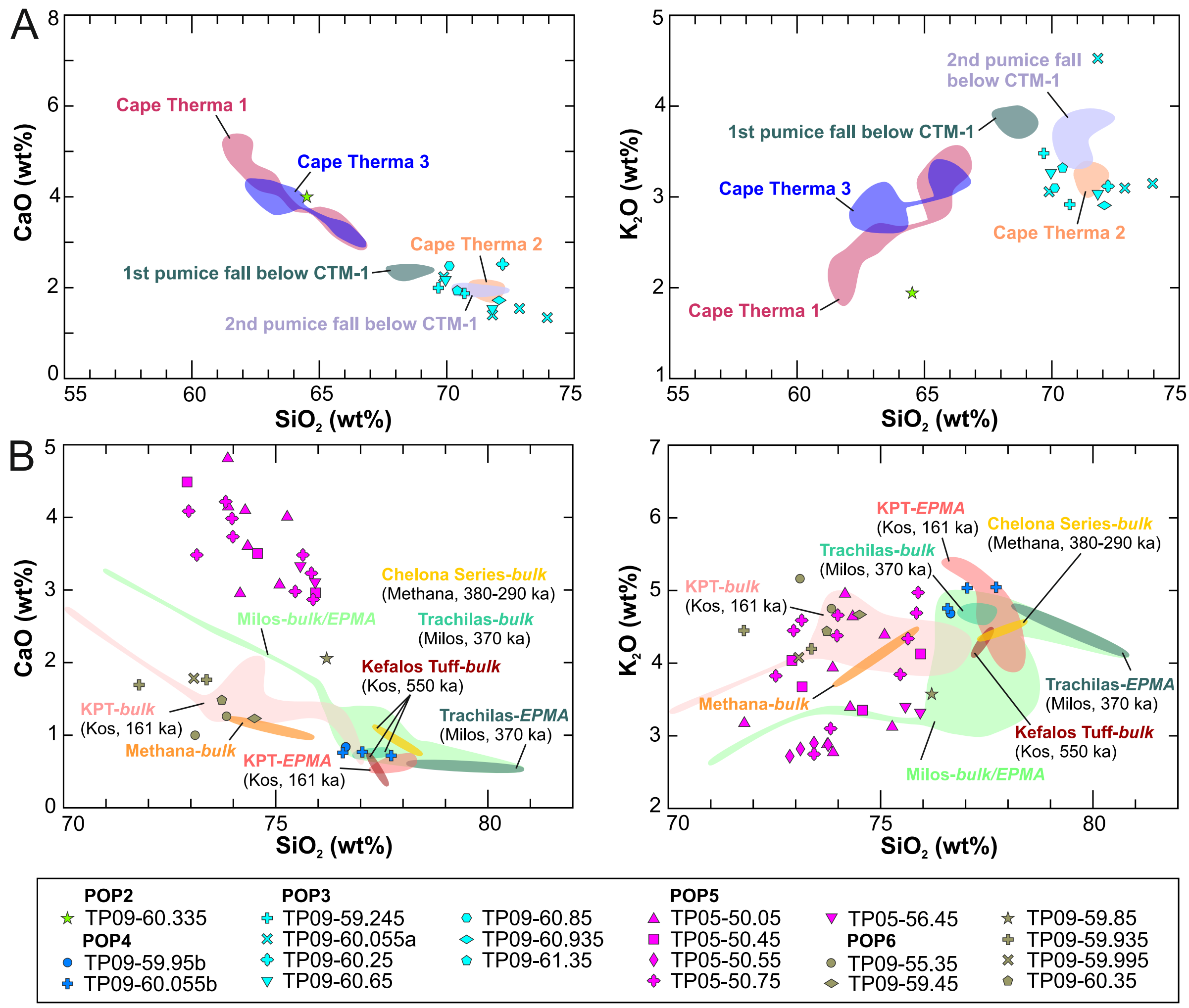

A
Cape Therma 1
Cape Therma 3
Cape Therma 2
1st pumice fall below CTM-1
2nd pumice fall below CTM-1
CaO (wt%)
SiO2 (wt%)
2nd pumice fall below CTM-1
1st pumice fall below CTM-1
Cape Therma 3
Cape Therma 2
Cape Therma 1
K2O (wt%)
B
Chelona Series-bulk
(Methana, 380-290 ka)
Milos-bulk/EPMA
Trachilas-bulk
(Milos, 370 ka)
Kefalos Tuff-bulk
(Kos, 550 ka)
Trachilas-EPMA
(Milos, 370 ka)
KPT-bulk
(Kos, 161 ka)
Methana-bulk
KPT-EPMA
(Kos, 161 ka)
KPT-EPMA
(Kos, 161 ka)
Chelona Series-bulk
(Methana, 380-290 ka)
Trachilas-bulk
(Milos, 370 ka)
KPT-bulk
(Kos, 161 ka)
Methana-bulk
Trachilas-EPMA
(Milos, 370 ka)
Kefalos Tuff-bulk
(Kos, 550 ka)
Milos-bulk/EPMA
POP2
TP09-60.335
POP4
TP09-59.95b
TP09-60.055b
POP3
TP09-59.245
TP09-60.055a
TP09-60.25
TP09-60.65
TP09-60.85
TP09-60.935
TP09-61.35
POP5
TP05-50.05
TP05-50.45
TP05-50.55
TP05-50.75
TP05-56.45
POP6
TP09-55.35
TP09-59.45
TP09-59.85
TP09-59.935
TP09-59.995
TP09-60.35

Figure 7

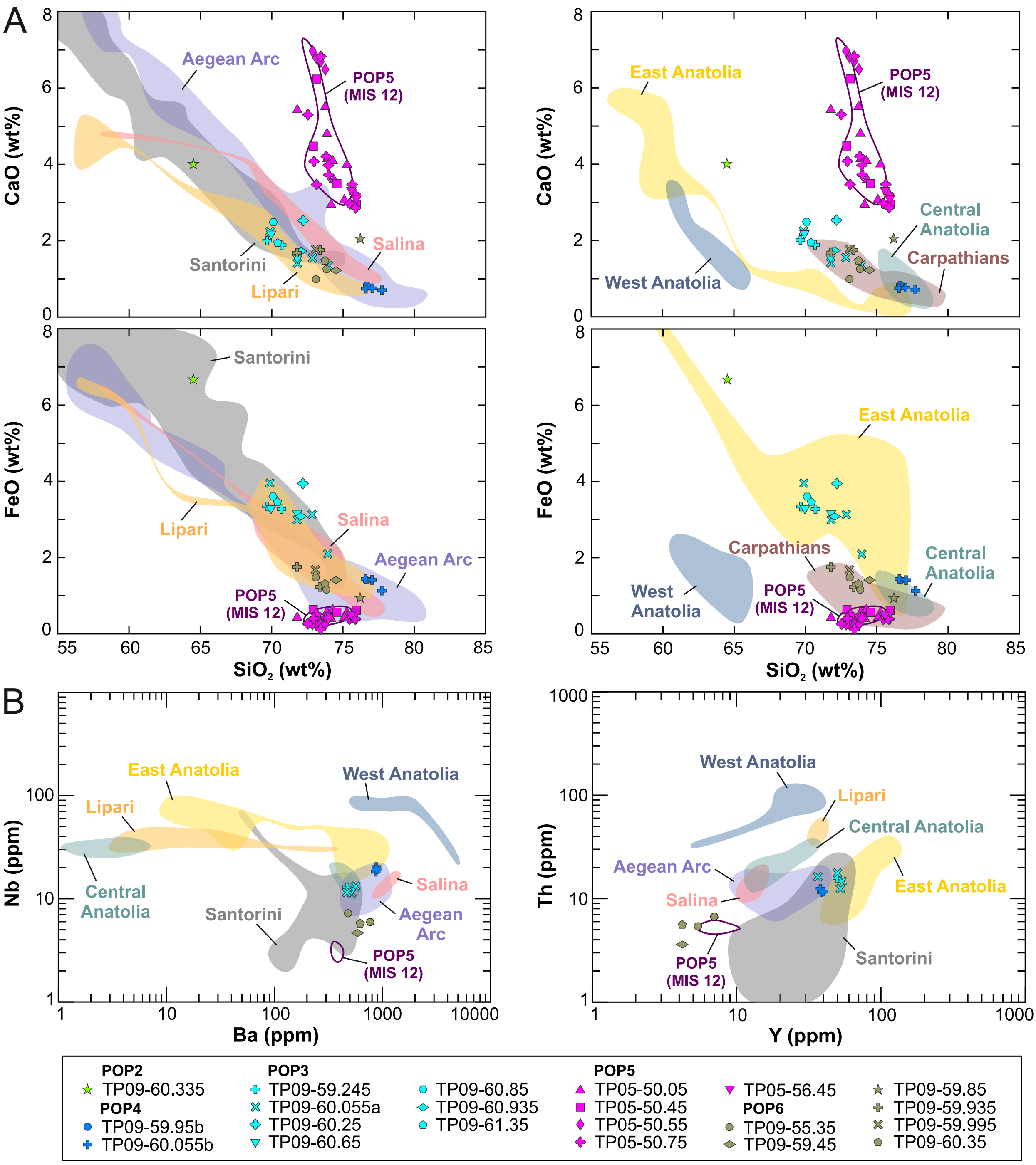

A
CaO (wt%)
FeO (wt%)
SiO2 (wt%)
Aegean Arc
POP5 (MIS 12)
Salina
Santorini
Lipari
East Anatolia
West Anatolia
Central Anatolia
Carpathians
B
Nb (ppm)
Ba (ppm)
Th (ppm)
Y (ppm)
POP2
TP09-60.335
POP4
TP09-59.95b
TP09-60.055b
POP3
TP09-59.245
TP09-60.055a
TP09-60.25
TP09-60.65
TP09-60.85
TP09-60.935
TP09-61.35
POP5
TP05-50.05
TP05-50.45
TP05-50.55
TP05-50.75
TP05-56.45
POP6
TP09-55.35
TP09-59.45
TP09-59.85
TP09-59.935
TP09-59.995
TP09-60.35

Table 1

Core	Tephra	TP-2005 depth range (m)	TP-2009 depth range (m)	Glass-shard counts per g dry weight	Number of analyzed shards	Geochemical population	Provenance	Age estimates (ka)	MIS
TP-2005	TP05-50.05	50.00–50.10		3	9	POP5	Unknown	235	7
TP-2005	TP05-50.45	50.40–50.50		1	4	POP5	Unknown	238	7
TP-2005	TP05-50.55	50.50–50.60		2	4	POP5	Unknown	239	7
TP-2005	TP05-50.75	50.70–50.80		24	11	POP5	Unknown	240	7
TP-2005	TP05-56.41	56.40–56.42	55.03–55.05	7	5	POP1A	Campanian Province, Seiano Ignimbrite?	289	9
TP-2009	TP09-55.045	56.41–56.42	55.04–55.05	2	1	POP1A	Campanian Province, Seiano Ignimbrite?	289	9
TP-2005	TP05-56.45	56.40–56.50		1	2	POP5	Unknown	289	9
TP-2005	TP05-56.475	56.47–56.48	55.09–55.10	10	3	POP1A	Campanian Province, Seiano Ignimbrite?	289	9
TP-2009	TP09-55.095	56.47–56.48	55.09–55.10	2	1	POP1A	Campanian Province, Seiano Ignimbrite?	289	9
TP-2009	TP09-55.195*		55.19–55.20	2	0	-	-	289	9
TP-2009	TP09-55.35		55.30–55.40	1	2	POP6	Aeolian Arc, Lipari?	290	9
TP-2009	TP09-57.45*		57.40–57.50	0.1	0	-	-	302	9
TP-2009	TP09-59.235		59.23–59.24	3	1	POP1C	Campanian Province	313	9
TP-2009	TP09-59.245		59.24–59.25	2	2	POP3	Santorini, M2 activities?	313	9
TP-2009	TP09-59.45		59.40–59.50	1	1	POP6	Aeolian Arc, Lipari?	314	9
TP-2009	TP09-59.85		59.80–59.90	0.2	1	POP6	Aeolian Arc, Lipari?	316	9
TP-2009	TP09-59.935		59.93–59.94	3	2	POP6	Aeolian Arc, Lipari?	316	9
TP-2009	TP09-59.95a		59.90–60.00	1	1	POP1A	Campanian Province	316	9
TP-2009	TP09-59.95b				1	POP4	Aegean Arc, Kos or Milos?	316	9
TP-2009	TP09-59.995		59.99–60.00	2	1	POP6	Aeolian Arc, Lipari?	317	9
TP-2009	TP09-60.05a		60.00–60.10	14	1	POP1A	Campi Flegrei, reworked CI	317	9
TP-2009	TP09-60.05b				7	POP1B	Campi Flegrei, reworked CI	317	9
TP-2009	TP09-60.055a		60.05–60.06	6	4	POP3	Santorini, M2 activities?	317	9
TP-2009	TP09-60.055b				3	POP4	Aegean Arc, Kos or Milos?	317	9

Core	Tephra	TP-2005 depth range (m)	TP-2009 depth range (m)	Glass-shard counts per g dry weight	Number of analyzed shards	Geochemical population	Provenance	Age estimates (ka)	MIS
TP-2009	TP09-60.25		60.20–60.30	0.4	1	POP3	Santorini, M2 activities?	318	9
TP-2009	TP09-60.335		60.33–60.34	4	1	POP2	Santorini, M2 activities?	318	9
TP-2009	TP09-60.35		60.30–60.40	1	1	POP6	Aeolian Arc, Lipari?	318	9
TP-2009	TP09-60.65		60.60–60.70	0.5	2	POP3	Santorini, M2 activities?	319	9
TP-2009	TP09-60.85		60.80–60.90	4	1	POP3	Santorini, M2 activities?	320	9
TP-2009	TP09-60.935		60.93–60.94	3	1	POP3	Santorini, M2 activities?	321	9
TP-2009	TP09-60.95*		60.90–61.00	1	0	-	-	321	9
TP-2009	TP09-61.335*		61.33–61.34	3	0	-	-	324	9
TP-2009	TP09-61.35		61.30–61.40	0.4	1	POP3	Santorini, M2 activities?	324	9
TP-2009	TP09-61.85*		61.80–61.90	0.4	0	-	-	328	9

Table 2

Tephra	TP05-50.05	TP06-50.45	TP05-50.55	TP05-50.75	TP05-56.41	TP09-55.045	TP05-56.45	TP05-56.475	TP09-55.095	TP09-55.35
Provenance	Unknown	Unknown	Unknown	Unknown	Campanian Province, Seiano Ign.?	Campanian Province, Seiano Ign.?	Unknown	Campanian Province, Seiano Ign.?	Campanian Province, Seiano Ign.?	Aeolian Arc?
(wt%)										
SiO_2	73.31	73.94	71.33	71.95	57.44	61.44	75.69	57.77	56.54	73.36
TiO_2	0.07	0.05	0.15	0.08	0.40	0.43	0.08	0.50	0.73	0.20
Al_2O_3	13.27	13.96	12.78	13.90	17.87	18.47	13.73	18.45	18.37	14.75
FeO	0.43	0.58	0.26	0.47	2.99	2.39	0.60	3.96	5.68	1.17
MnO	0.00	0.01	0.00	0.00	0.14	0.16	0.00	0.13	0.13	0.02
MgO	2.75	1.89	3.04	1.98	0.69	0.33	1.64	1.08	1.95	2.19
CaO	5.47	3.47	6.62	3.63	2.52	1.89	3.10	3.32	4.38	1.26
Na_2O	1.20	1.92	0.58	0.67	3.61	4.39	1.49	3.53	3.12	1.59
K_2O	2.87	3.33	2.76	4.53	9.01	7.32	3.32	8.49	7.69	4.72
P_2O_5	0.05	0.01	0.04	0.04	0.06	0.03	0.03	0.14	0.30	0.09
F	0.00	0.00	0.00	0.00	0.00	0.03	0.00	0.00	0.00	0.00
Cl	0.01	0.01	0.01	0.02	0.53	0.66	0.00	0.58	0.54	0.01
Total	99.42	99.18	97.57	97.26	95.27	97.50	99.68	97.95	99.43	99.37
(ppm)										
Rb										134.5
Sr										48.4
Y										5.4
Zr										19.9
Nb										7.3
Ba										475.7
La										21.9
Ce										40.9
Th										5.4
U										2.0

Table 2 continued

Tephra	TP09-59.235	TP09-59.245	TP09-59.45	TP09-59.85	TP09-59.935	TP09-59.95a	TP09-59.95b	TP09-59.995	TP09-60.05a	TP09-60.05b
Provenance	Campanian Province	Santorini	Aeolian Arc?	Aeolian Arc?	Aeolian Arc?	Campanian Province	Aegean Arc, Kos or Milos?	Aeolian Arc?	Campi Flegrei, reworked CI	Campi Flegrei, reworked CI
(wt%)										
SiO_2	59.85	66.31	72.66	75.22	71.42	60.82	75.36	72.48	61.18	62.32
TiO_2	0.37	0.45	0.11	0.12	0.15	0.37	0.10	0.08	0.40	0.42
Al_2O_3	19.31	14.14	12.99	13.12	16.09	18.45	13.01	14.12	18.58	18.92
FeO	2.92	3.08	1.40	0.95	1.76	3.26	1.40	1.69	3.45	2.85
MnO	0.13	0.13	0.02	0.01	0.04	0.13	0.03	0.00	0.07	0.20
MgO	0.57	0.49	3.05	2.73	2.41	0.77	0.03	3.62	0.80	0.32
CaO	1.43	1.78	1.20	2.03	1.69	1.68	0.83	1.78	2.64	1.19
Na_2O	7.08	4.58	1.50	0.96	1.44	4.38	2.95	1.34	3.32	5.50
K_2O	4.84	2.74	4.55	3.53	4.43	7.74	4.60	4.05	9.21	7.27
P_2O_5	0.11	0.09	0.06	0.05	0.07	0.12	0.00	0.05	0.19	0.00
F	0.00	0.00	0.00	0.00	0.00	0.00	0.00	0.00	0.00	0.00
Cl	0.45	0.24	0.01	0.02	0.01	0.37	0.11	0.00	0.35	0.72
Total	97.04	94.05	97.53	98.73	99.51	98.10	98.42	99.20	100.18	99.71
(ppm)										
Rb	186.6	92.0	134.6			227.7			237.7	369.2
Sr	111.6	70.7	67.9			373.8			615.8	16.5
Y	23.0	49.9	4.2			20.4			19.9	55.1
Zr	228.4	328.7	17.1			182.9			176.6	672.4
Nb	39.1	12.9	4.7			28.9			27.8	118.2
Ba	54.8	467.5	580.9			360.6			808.2	19.1
La	52.4	25.7	20.4			42.3			42.7	125.1
Ce	94.4	56.5	38.0			79.2			80.8	239.3
Th	16.5	15.8	3.6			13.3			12.4	50.6
U	5.7	5.3	1.7			4.8				18.2

Table 2 continued

Tephra	TP09-60.055a	TP09-60.055b	TP09-60.25	TP09-60.335	TP09-60.35	TP09-60.65	TP09-60.85	TP09-60.935	TP09-61.35
Provenance	Santorini	Aegean Arc, Kos or Milos?	Santorini	Santorini	Aeolian Arc?	Santorini	Santorini	Santorini	Santorini
(wt%)									
SiO_2	73.18	77.00	66.32	63.63	73.52	70.65	66.00	72.06	66.27
TiO_2	0.46	0.08	0.55	0.88	0.06	0.46	0.51	0.42	0.45
Al_2O_3	15.05	12.59	14.20	15.38	13.75	14.35	14.11	14.62	14.45
FeO	3.15	1.14	3.63	6.57	1.32	3.13	3.40	3.09	3.26
MnO	0.06	0.05	0.10	0.18	0.00	0.15	0.08	0.13	0.15
MgO	0.41	0.05	0.65	1.42	3.43	0.45	0.62	0.43	0.56
CaO	1.58	0.72	2.33	3.95	1.49	1.55	2.35	1.75	1.84
Na_2O	3.38	2.41	1.12	4.45	1.66	4.60	4.07	4.53	3.94
K_2O	3.11	4.99	2.87	1.93	4.43	2.99	2.92	2.91	3.12
P_2O_5	0.07	0.03	0.11	0.26	0.05	0.08	0.09	0.08	0.08
F	0.00	0.00	0.00	0.00	0.00	0.00	0.00	0.00	0.00
Cl	0.28	0.10	0.19	0.23	0.01	0.24	0.19	0.26	0.24
Total	100.73	99.17	92.07	98.85	99.72	98.66	94.34	100.28	94.36
(ppm)									
Rb	104.0	136.7			115.3				
Sr	74.7	37.2			72.0				
Y	52.4	39.9			4.2				
Zr	317.2	133.9			15.7				
Nb	11.6	19.4			5.8				
Ba	463.8	871.6			615.8				
La	25.2	31.7			17.8				
Ce	54.5	65.2			33.0				
Th	12.5	11.7			5.6				
U	3.7	3.7			1.1				

Supplement 2

Table S1: Tie points used in the Si-based alignment of cores TP-2005 and TP-2009. Software: AnalySeries (Paillard et al., 1996).

TP-2009 Depth (m)	TP-2005 Depth (m)	Offset (m)	Temporal offset (ka)
50.44	51.06	0.62	4.98
51.39	52.28	0.88	10.15
51.72	52.94	1.22	13.34
52.97	53.97	1.00	7.26
53.62	54.69	1.06	7.71
55.10	56.48	1.38	8.43
55.60	56.64	1.04	6.35
56.34	57.40	1.06	7.23
57.51	58.35	0.84	6.06
57.92	59.01	1.08	7.61
58.45	59.81	1.35	7.94

Table S2: Tie points used for the alignment of the tree-pollen record from core TP-2009 to that from the old Tenaghi Philippon core TF-II (Wijmstra and Smit, 1976; Van der Wiel and Wijmstra, 1987) for the 460–335 ka (Vakhrameeva et al., 2018) and 335–312 ka (this study) intervals using the orbitally tuned age model of Tzedakis et al. (2006). Software: AnalySeries (Paillard et al., 1996).

TP-2009 Depth (m)	TF-II Age (ka)
59.23	312.22
59.52	314.51
60.04	316.68
60.77	319.85
63.15	336.85
64.63	349.07
66.60	364.04
67.98	376.61
68.57	379.50
75.54	423.39
75.98	430.00
76.64	433.06
78.71	440.43
79.84	446.69
80.79	452.88
81.67	455.78
81.90	458.00

References

Paillard, D., Labeyrie, L., Yiou, P., 1996. Macintosh Program performs time-series analysis. Eos, Transactions, American Geophysical Union 77, 379-379.

Tzedakis, P.C., Hooghiemstra, H., Pälike, H., 2006. The last 1.35 million years at Tenaghi Philippon: revised chronostratigraphy and long-term vegetation trends. Quaternary Science Reviews 25, 3416-3430.

Vakhrameeva, P., Koutsodendris, A., Wulf, S., Fletcher, W.J., Appelt, O., Knipping, M., Gertisser, R., Trieloff, M., Pross, J., 2018. The cryptotephra record of the Marine Isotope Stage 12 to 10 interval (460–335 ka) at Tenaghi Philippon, Greece: Exploring chronological markers for the Middle Pleistocene of the Mediterranean region. Quaternary Science Reviews 200, 313-333.

Van der Wiel, A.M., Wijmstra, T.A., 1987. Palynology of the lower part (78–120 m) of the core Tenaghi Philippon II, Middle Pleistocene of Macedonia, Greece. Review of Palaeobotany and Palynology 52, 73-88.

Wijmstra, T.A., Smit, A., 1976. Palynology of the middle part (30–78 metres) of the 120 m deep section in northern Greece (Macedonia). Acta Botanica Neerlandica 25, 297-312.

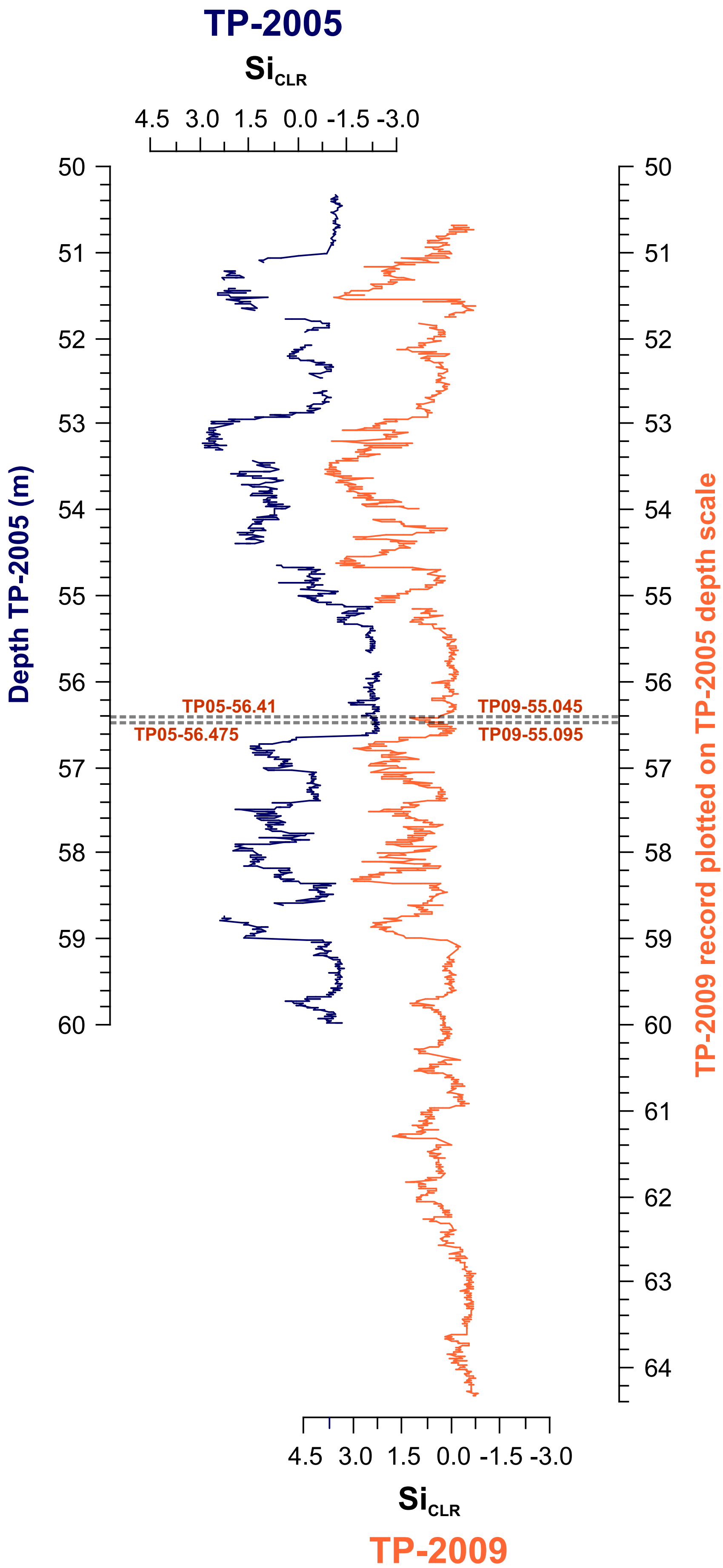

Figure S1: Normalized Si_{CLR} records for the overlap intervals of the Tenaghi Philippon cores TP-2005 and TP-2009 after core alignment. Dashed lines mark cryptotephra layers that are present in both cores.

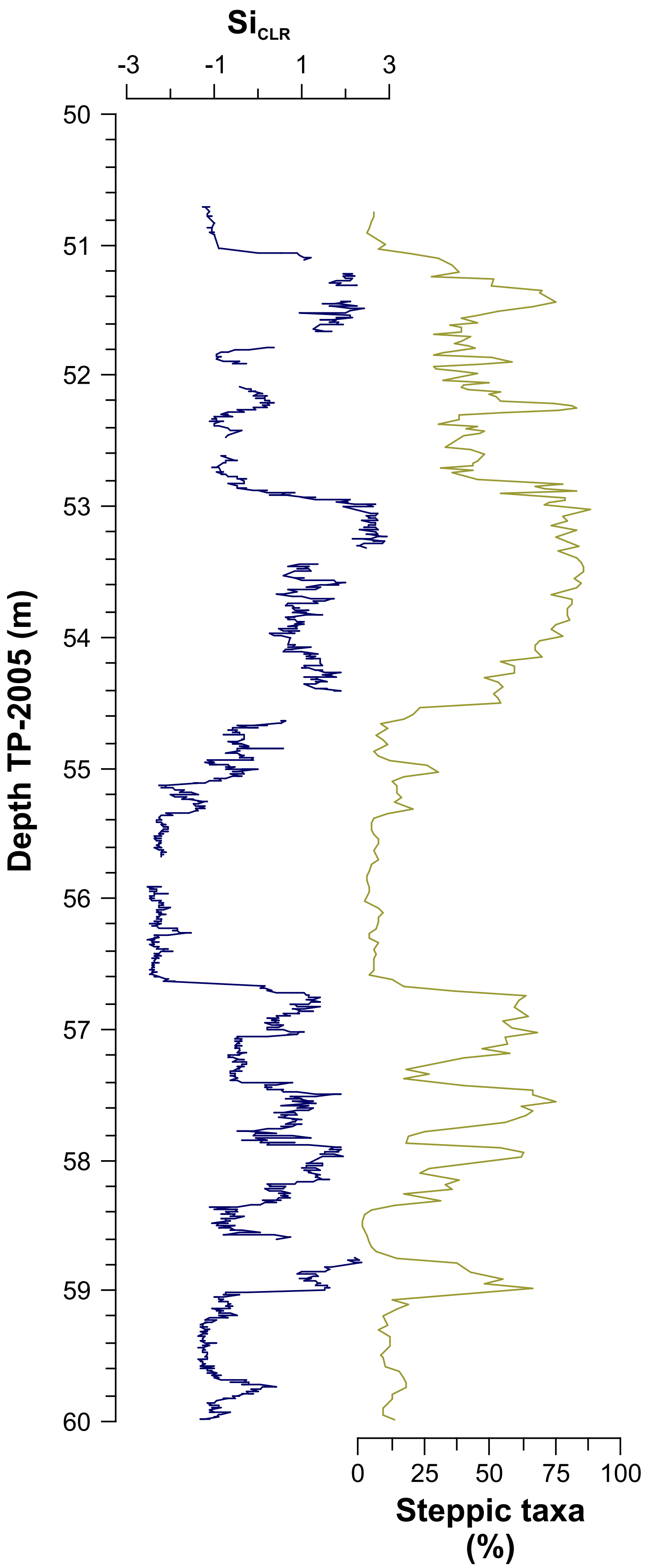

Figure S2: Comparison of normalized Si_{CLR} intensities and percentages of steppic taxa in the 60–50 m interval of core TP-2005.

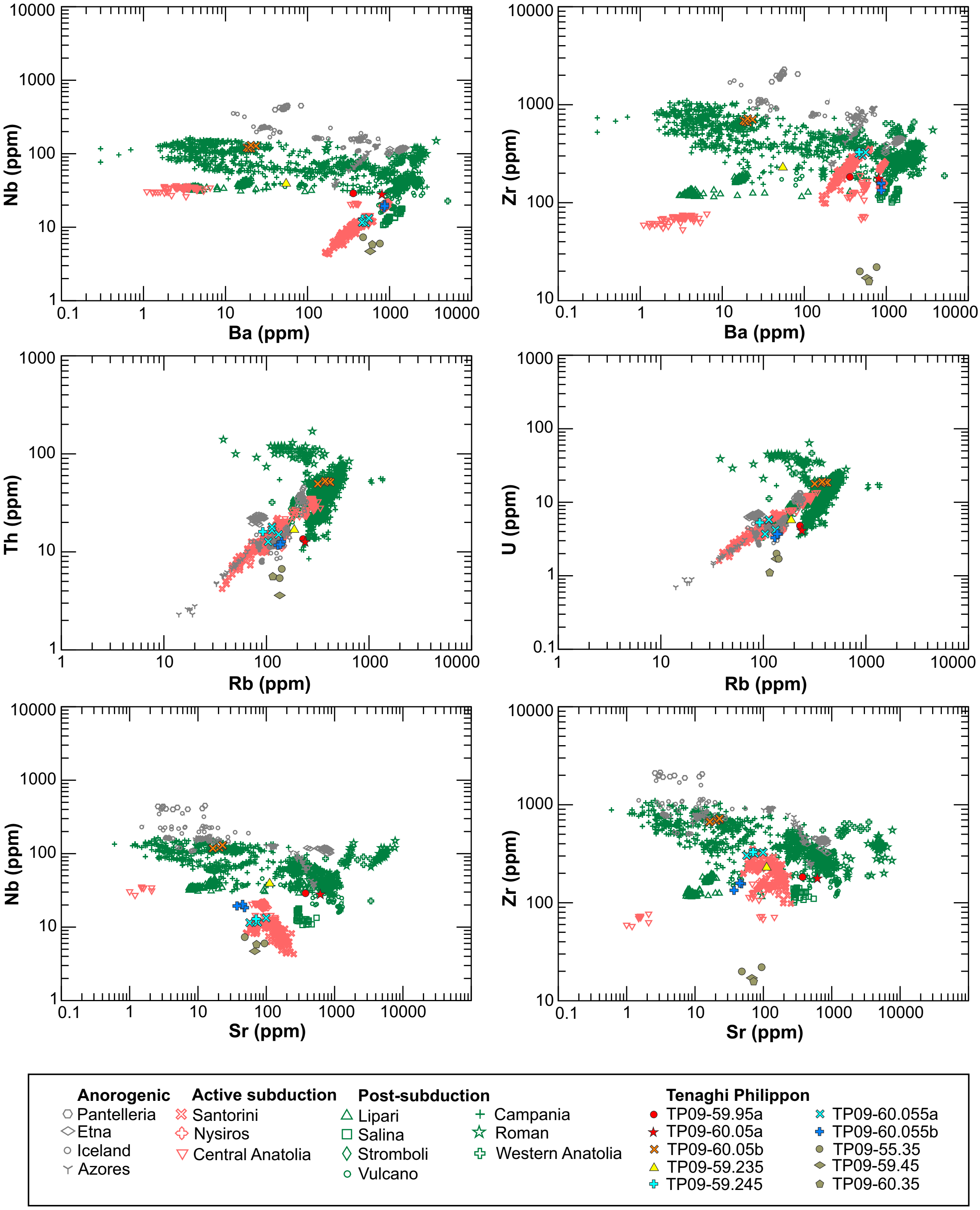

Figure S3: Complementary trace-element plots to Fig. 4 in the text.

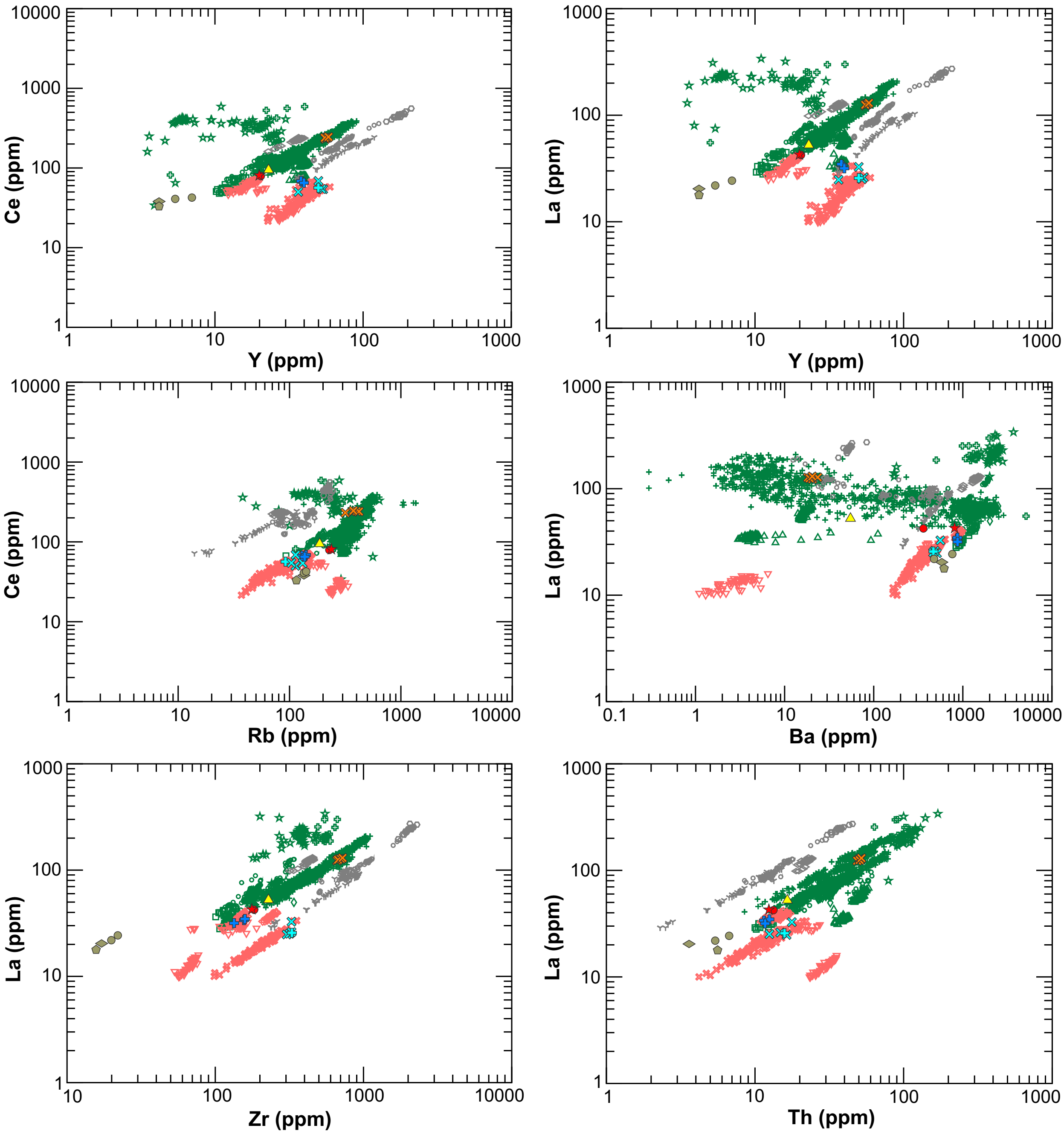

Figure S3: *(continued)*.

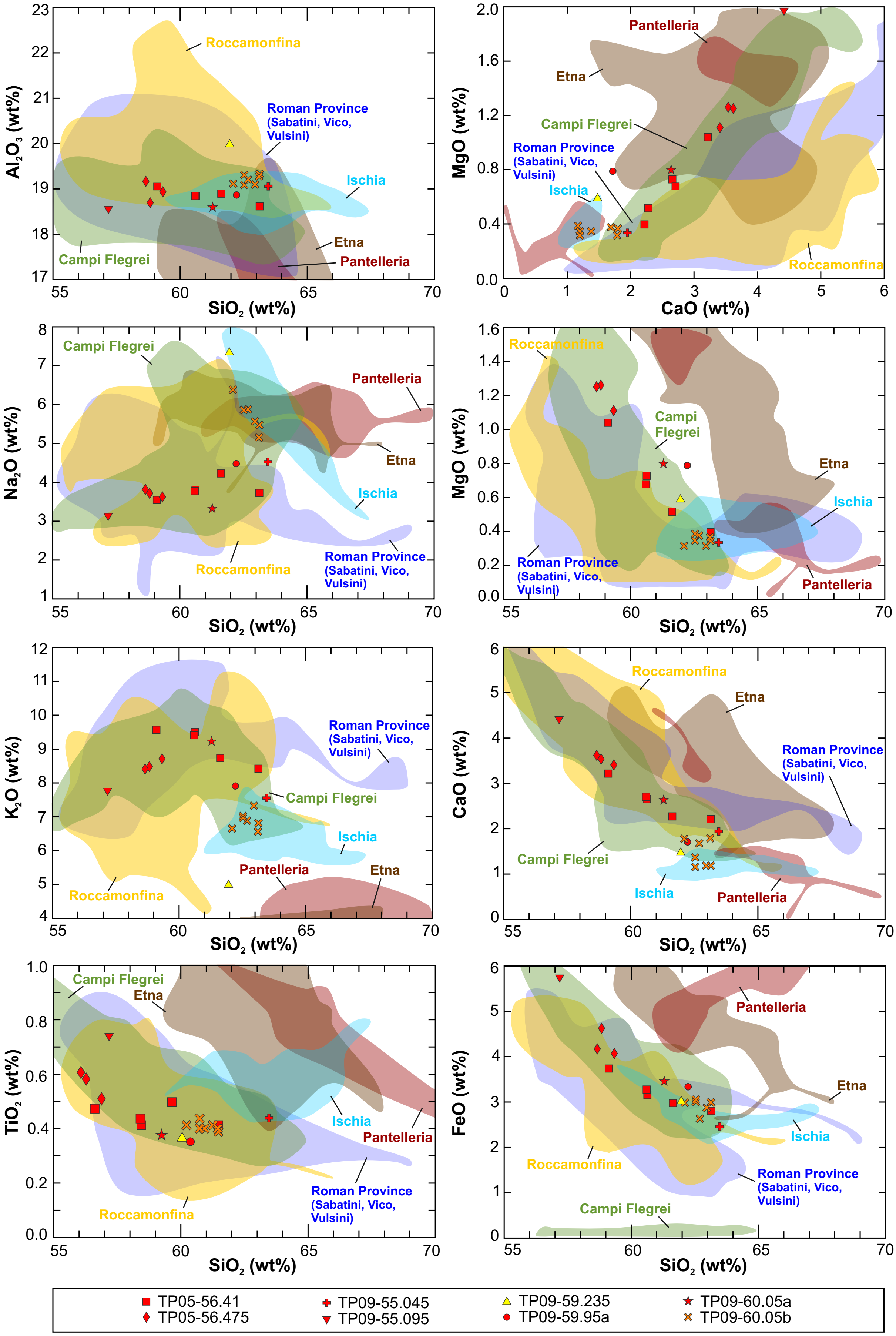

Figure S4: Complementary major- and trace-element plots to Fig. 5 in the text.

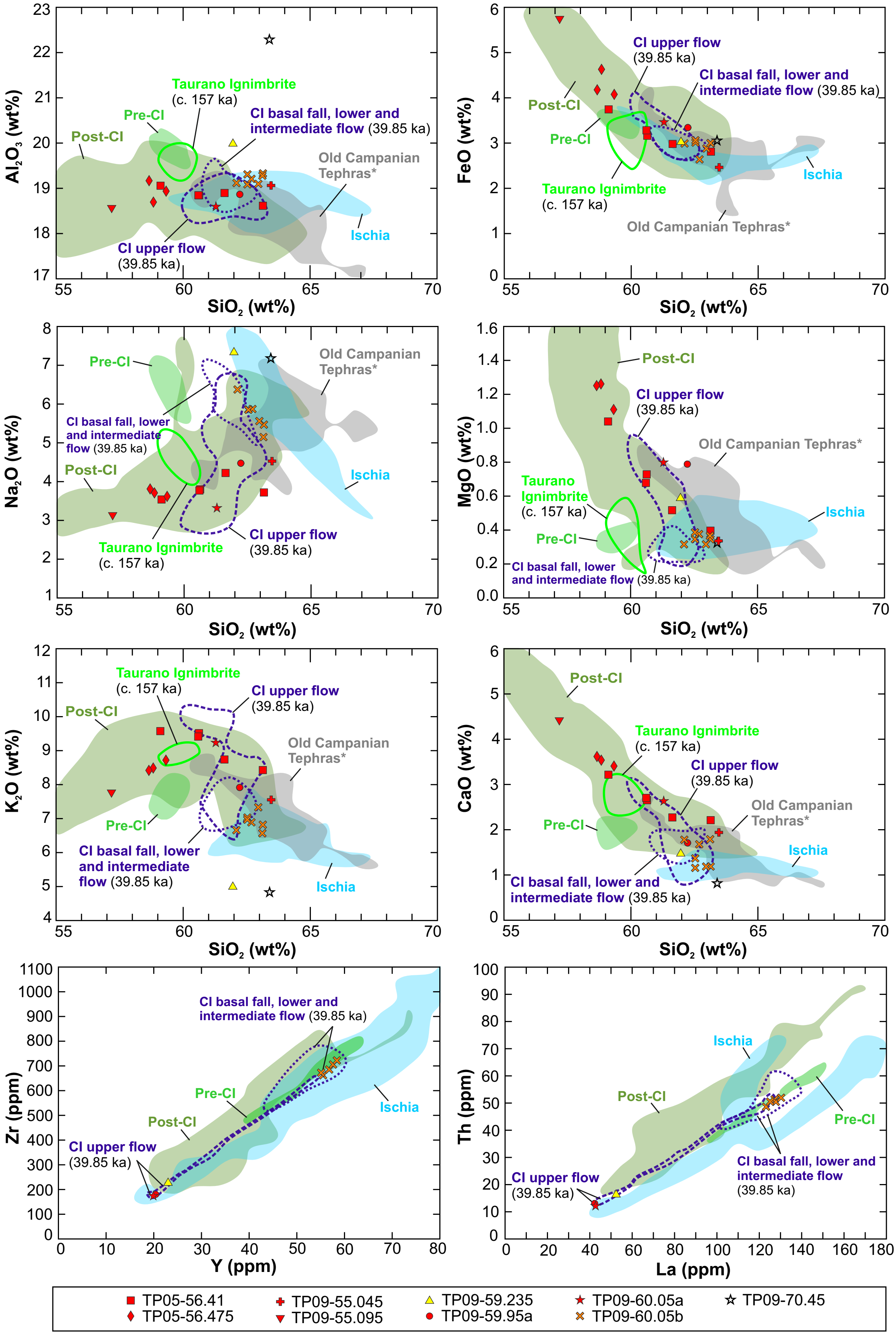

Figure S4: *(continued).*

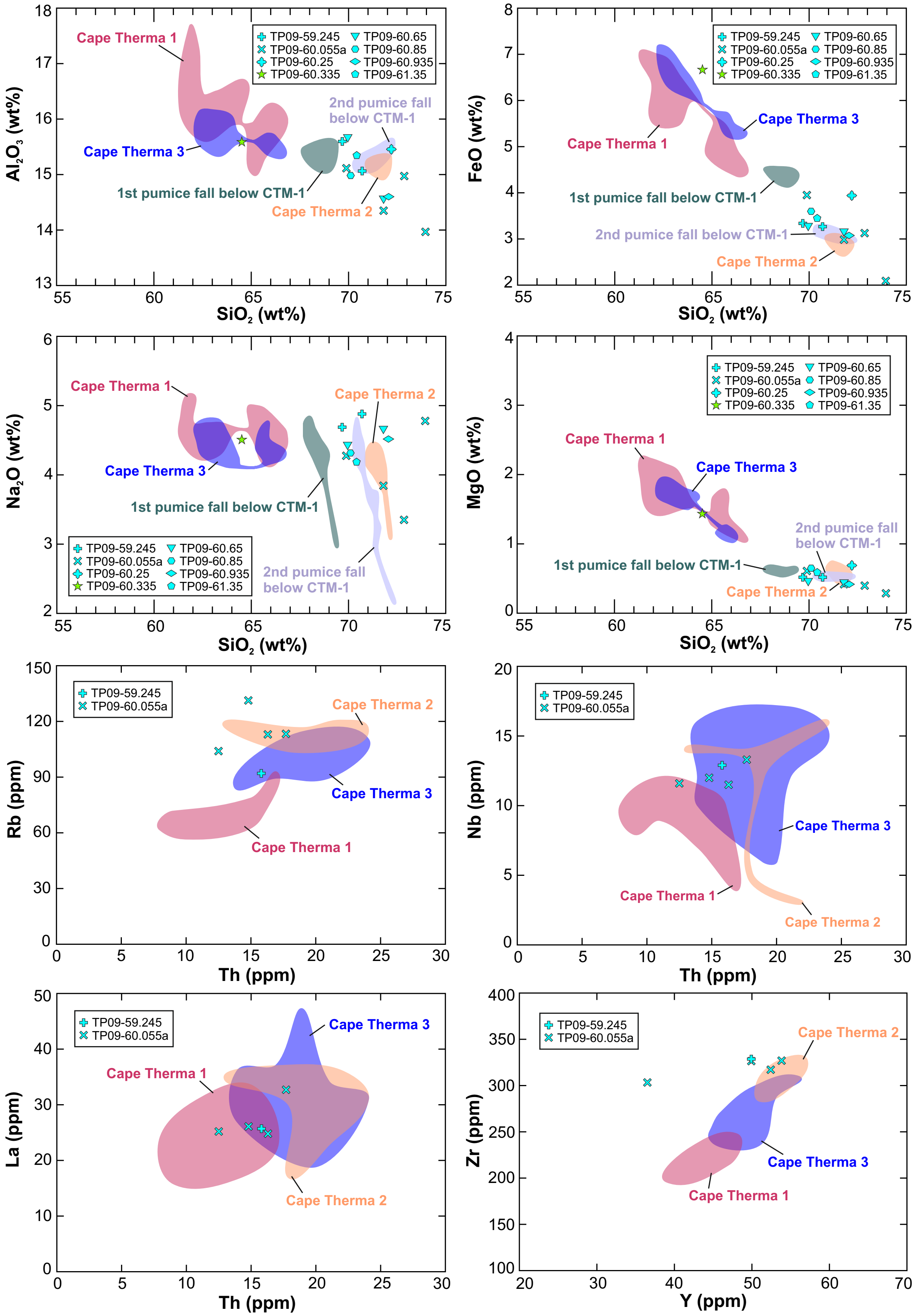

Figure S5: Complementary major- and trace-element plots to Fig. 6 in the text.

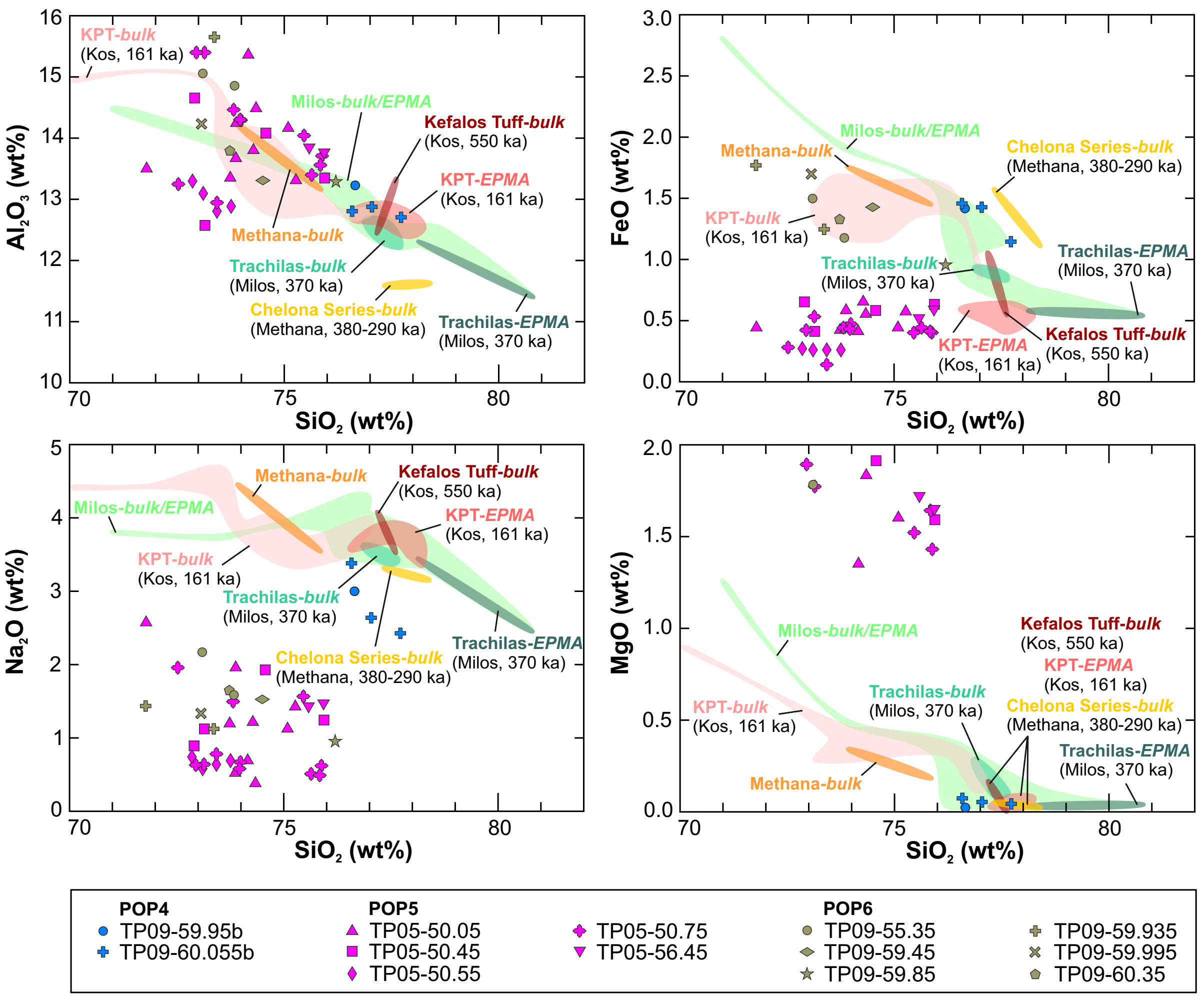

Figure S5: (*continued*).

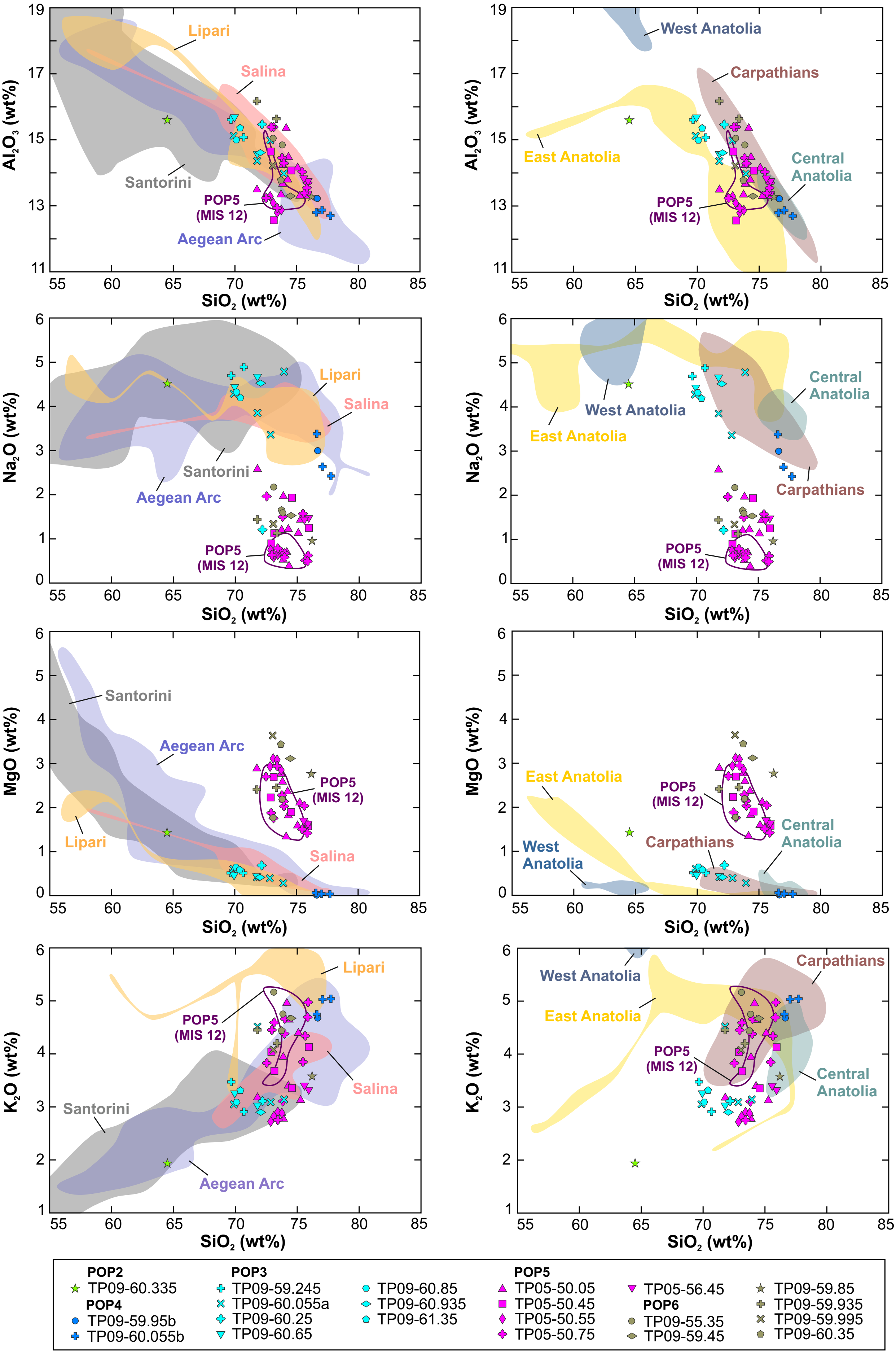

Figure S6: Complementary major- and trace-element plots to Fig. 7 in the text.

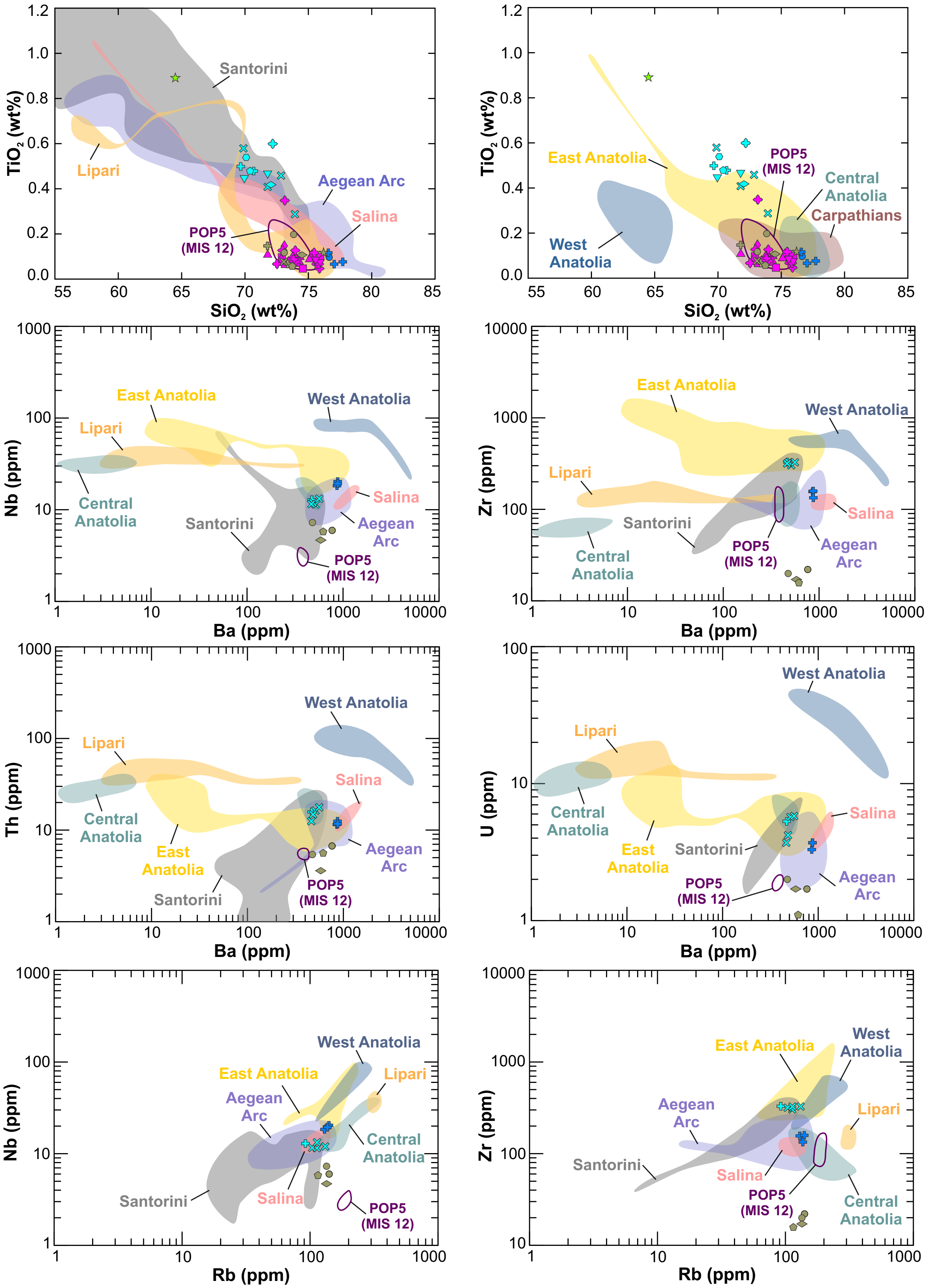

Figure S6: (*continued*).

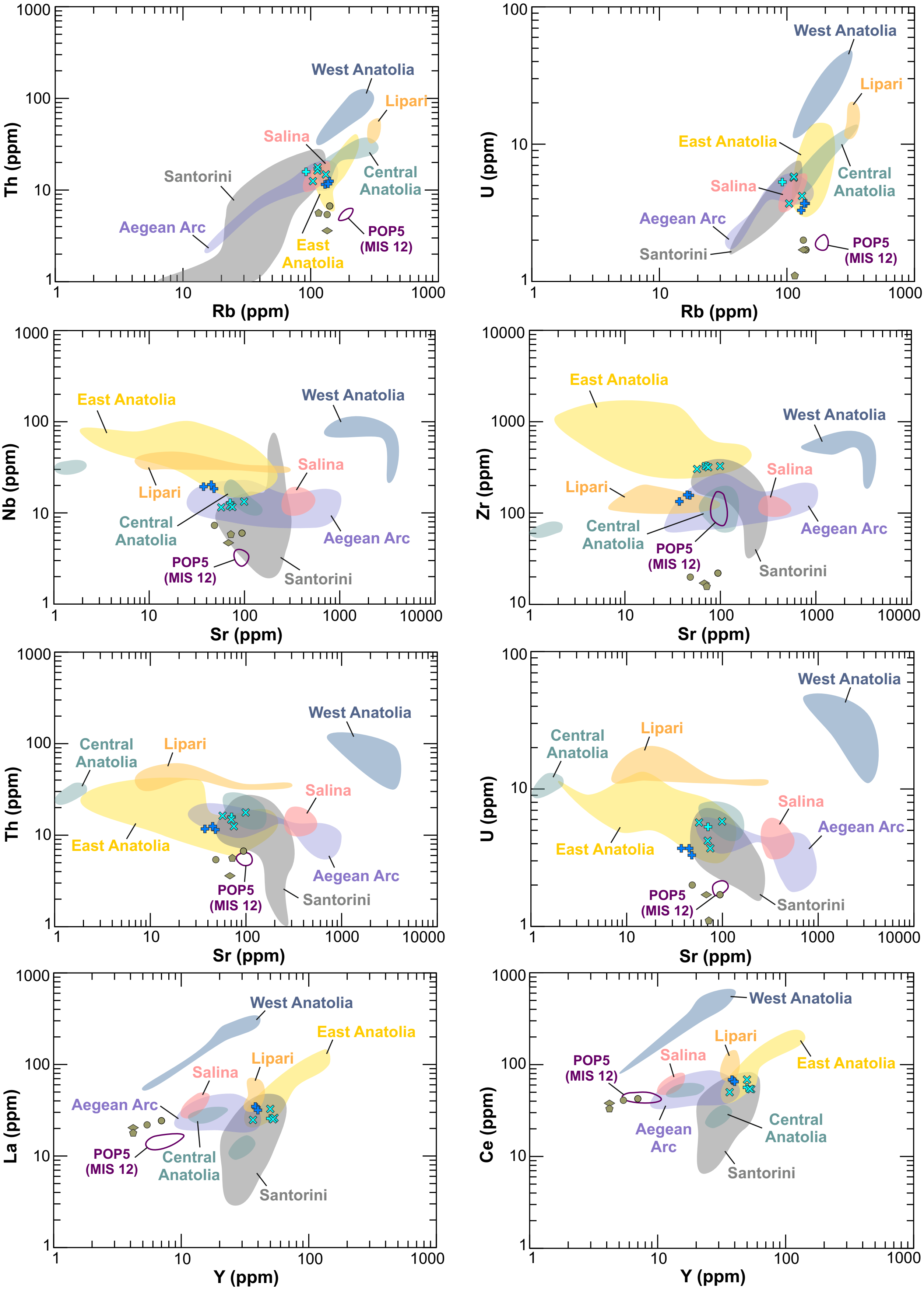

Figure S6: (*continued*).

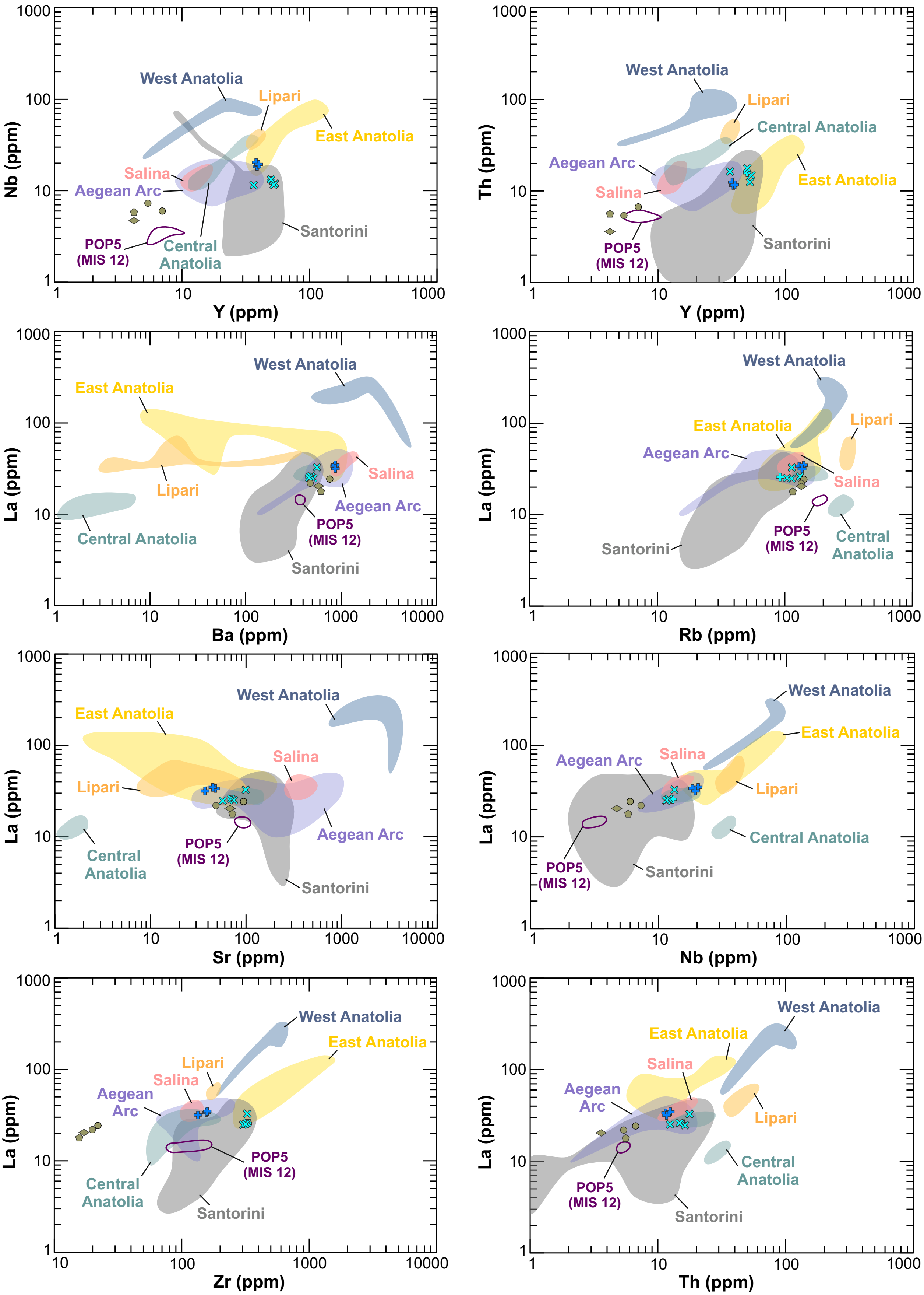

Figure S6: (*continued*).